

This is to certify that the

thesis entitled

A Strain Study in the Kona Formation, Marquette County, Michigan

presented by

Rudolf Meyer

has been accepted towards fulfillment of the requirements for

Masters degree in Geology

Date 04/29/83

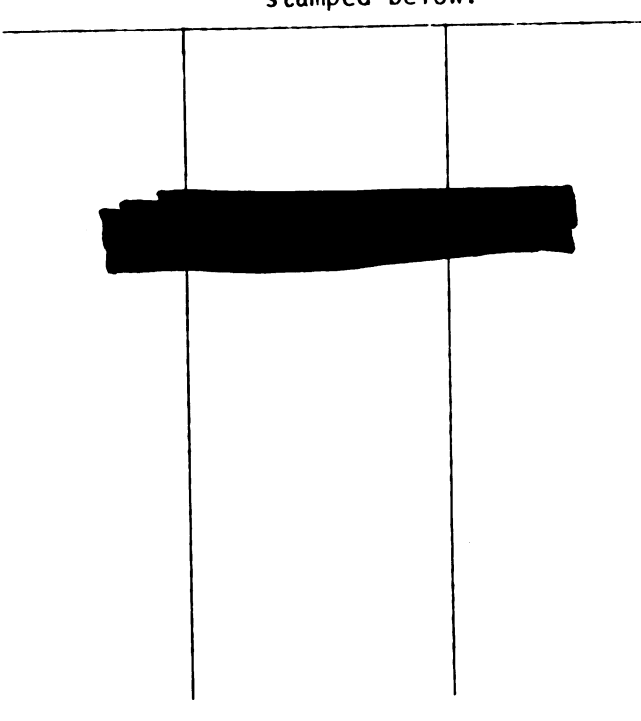
MSU is an Affirmative Action/Equal Opportunity Institution

O-7639



RETURNING MATERIALS:

Place in book drop to remove this checkout from your record. FINES will be charged if book is returned after the date stamped below.



A STRAIN STUDY IN THE KONA FORMATION, MARQUETTE COUNTY, MICHIGAN

by

Rudolf Meyer

A THESIS

Submitted to
Michigan State University
in partial fulfillment of the requirements
for the degree of

MASTER OF SCIENCE

Department of Geology

1983

ABSTRACT

A STRAIN STUDY IN THE KONA FORMATION, MARQUETTE COUNTY, MICHIGAN

by

Rudolf Meyer

Argillites and slates of the Kona Formation contain reduction spots which are the quantitative strain markers used in this study. At the locality, on the southern margin of the eastern Marquette Trough, flat-lying argillite and folded slate contain reduction spots with long axes subparallel to and at high angles to bedding, respectively.

Reduction spot finite strains were calculated for both domains. For comparison, the quartz grain shape fabric in adjacent quartzites was analyzed to obtain a semi-quantitative measure of strain.

Modelling based on reduction spot strains results in the following sequence:
1) 40% compaction of initially spherical "spots"; 2) 30% layer-parallel flattening
prior to folding; and 3) folding by additional pure shear and simple shear oblique
to bedding.

The quartz grain shapes do not record strains comparable to that of the "spots". The implications of this study for models of cleavage development and the deformation history of the Marquette Trough are discussed.

ACKNOWLEDGEMENTS

Special thanks to Dr. Bill Cambray for inspiring my interest in structural geology and guidance during the thesis research. I am grateful to Steve Mattson, Dave Cladas and Bill Monaghan for their assistance, suggestions and patient listening during discussions. Thanks to Dr. David M. Miller for kindly providing me with the computer program.

TABLE OF CONTENTS

LIST OF FIGURES iv
LIST OF TABLES vi
INTRODUCTION
GEOLOGIC SETTING
Regional
Local
DESCRIPTION OF SAMPLES
Sample Sites
Cleavages
Petrographic Descriptions
Argillite and Slate
Reduction Spots
Quartzite
ANALYSIS: ASSUMPTIONS AND METHODOLOGY
Finite Strain from the Quartz Grain Shape Fabric
in Quartzites
Finite Strain from Reduction Spots
Models of Progressive Deformation Based on Reduction
Spot Finite Strain States
RESULTS AND DISCUSSION
Finite Strains from the Quartz Grain Shape Fabric
in Quartzites
Finite Strains from Reduction Spots
Model of Progressive Deformation Based on Reduction Spots 45
Compaction
—
Flat-lying (LQ-6-2 to folded LQ-1-9)
Folded (LQ-1-9 to LQ-1-6)
Implications of the Model for Progressive Cleavage
Development
Implications for the Deformation of the Marquette Trough 56
••••••••••••••••••••••••••••••••••••••
CONCLUSIONS
REFERENCES
APPENDIX

LIST OF FIGURES

Figure 1.	Location map of Upper Peninsula of Michigan and Marquette Trough
Figure 2.	Location map of study area within Marquette Trough
Figure 3.	Photograph of flat-lying argillite containing reduction spots
Figure 4.	Photograph of folded slate containing reduction spots
Figure 5.	Pace-and-compass map of study area
Figure 6.	Stereonet plot of poles to bedding, spaced cleavage and joints (high-strain zones excluded) 14
Figure 7.	Stereonet plot of poles to bedding, spaced cleavage and faults (high-strain zones)
Figure 8.	Optical micrograph of slate perpendicular to slaty cleavage and bedding (crossed polars)
Figure 9.	Optical micrograph of slate approximately parallel to slaty cleavage (crossed polars)
Figure 10.	Rose diagram of the orientation of long axes of grains in the bedding (horizontal) in flat-lying argillite
Figure 11.	Optical micrograph of reduction spot boundary in slate (uncrossed polars)
Figure 12.	Optical micrograph of deformed quartzite 23
Figure 13.	Method of adjusting principal elongations for pure shear
Figure 14.	Method of adjusting principal elongations for simple shear
Figure 15.	Polar plot of quartz grain shape fabric in flat-lying quartzite (LQ-6-2)
Figure 16.	Polar plot of quartz grain shape fabric in tilted uartzite (LQ-2-1)

LIST OF FIGURES (Continued)

Figure 17.	Stereonet plot for principal strain axes for flat-lying argillites	3
Figure 18.	Stereonet plot of principal strain axes, bedding, cleavages and lineations for folded slate (LQ-1-9)	•
Figure 19.	Stereonet plot of principal strain axes, bedding, cleavages and lineations for folded slate (LQ-1-6))
Figure 20.	Plot of mean axes ratio of reduction spot data planes versus the range in orientations of the long axis (D1)	l
Figure 21.	Rose diagram of the orientation of long axes of reduction spots parallel to bedding in flat-lying argillite (LQ-6-10)	4
Figure 22.	Stereonet plot of modelled shear planes and directions	3
Figure 23.	Diagram illustrating the relationship between the modelled shear and microbuckles	•
Figure 24.	Schematic diagram of the progressive deformation of reduction spots from flat-lying to folded layers 51	i
Figure 25.	Graph of measured and implied reduction spot finite strain states	3
Figure 26.	Schematic diagram illustrating the kinematics of the hypothetical model for the formation of a crenulation cleavage	5

LIST OF TABLES

Table 1.	Strain parameters from the quartz grain shape fabric in the quartzites	33
Table 2.	Strain parameters from reduction spots in argillite and slate	37
Table 3.	Strain components for the deformation increments modelled	52

INTRODUCTION

The measurement of finite strain in deformed rocks is dependent upon finding strain markers of known (i.e., measurable) original orientation and shape. Strain markers that have been used include onlites, pisolites, reduction spots, pebbles and fossils. Problems which arise with the quantitative measurement of strain markers are: 1) that the original shape and orientation of the markers are not known with certainty, and 2) rarely are undeformed rocks containing the same strain markers found in close relationship to their deformed equivalents.

Graphical and algebraic methods of finite strain analysis therefore require the assumption of: a) initially spherical particles or a random distribution, or b) the identification from the deformed material of an initially symmetric shape fabric about some known plane (Ramsay, 1967; Elliott, 1970; Dunnet et al., 1971; Matthews et al., 1974; Shimamoto et al., 1976; Oertel, 1978; Miller et al., 1979; Siddans, 1980). The influence of initial fabrics with regard to strain analyses has been discussed by Boulter (1976), Seymour et al. (1979), Lisle (1979) and Holst (1982). The key analytical problem is the separation of compactional from tectonic strains.

In addition to orientation and shape, strain analyses require the evaluation of assumptions regarding the behaviour of the markers. Primarily, these assumptions are homogeneity of strain at the scale considered, constraints on the magnitude of volume changes and the effects of viscosity contrasts between the marker and the matrix.

Reduction spots in argillite and slate are the quantitative strain markers used in this study. They are yellow, pale orange, light green bodies of typically spherical to ellipsoidal shapes, believed to have formed during diagenesis under

locally reducing conditions (Miller et al., 1955; Ramsay, 1967). Wood (1973), Tullis et al. (1975) and Wood et al. (1980) state that it has been "demonstrated that these bodies are of diagenetic origin, were present prior to deformation, and were initially spherical in form". In their analyses they "... exclusively consider those ellipsoids for which initial sphericity had been ascertained".

Wood et al. (1980) do not present chemical data but indicate that the "spots" are depleted in iron content with respect to the matrix while maintaining the same oxidation state. Though a comprehensive study is clearly necessary, it is apparent that the reduction spots are almost identical to the matrix mineralogically (i.e., mimimum viscosity contrast) rendering them especially amenable for strain analysis. Several strain studies involving reduction spots have relied on the assumption that the slaty cleavage represents the XY-plane of the finite strain ellipsoid and have constrained the XY-plane of the "spots" to be parallel to the slaty cleavage (Wood, 1973, 1974; Tullis et al., 1975; Westjohn, 1978; Wood et al., 1980).

The study area is located within a small portion of the Marquette Trough in the Kona Formation of upper Michigan (Figures 1 and 2). Reduction spots occur in argillite and slate in a variety of shapes and orientations on any given plane. Almost all of these planar sections approximate an elliptical shape. The locality includes both flat-lying argillite without cleavage and tilted slates with a weakly developed slaty cleavage.

On the outcrop, it is clear that the reduction spots are flattened subparallel to bedding in the flat-lying argillites and make a steep angle with bedding in the folded slates (Figures 3 and 4). Thus, from field evidence alone it is suggested that the reduction spots at this locality record both compactional strain and tectonic strains superimposed on this initial fabric.



Figure 1. Location map of Upper Peninsula of Michigan and Marquette Trough.

Figure 2. Location map of study area within Marquette Trough. Dashed line shows areal extent of Kona Formation.

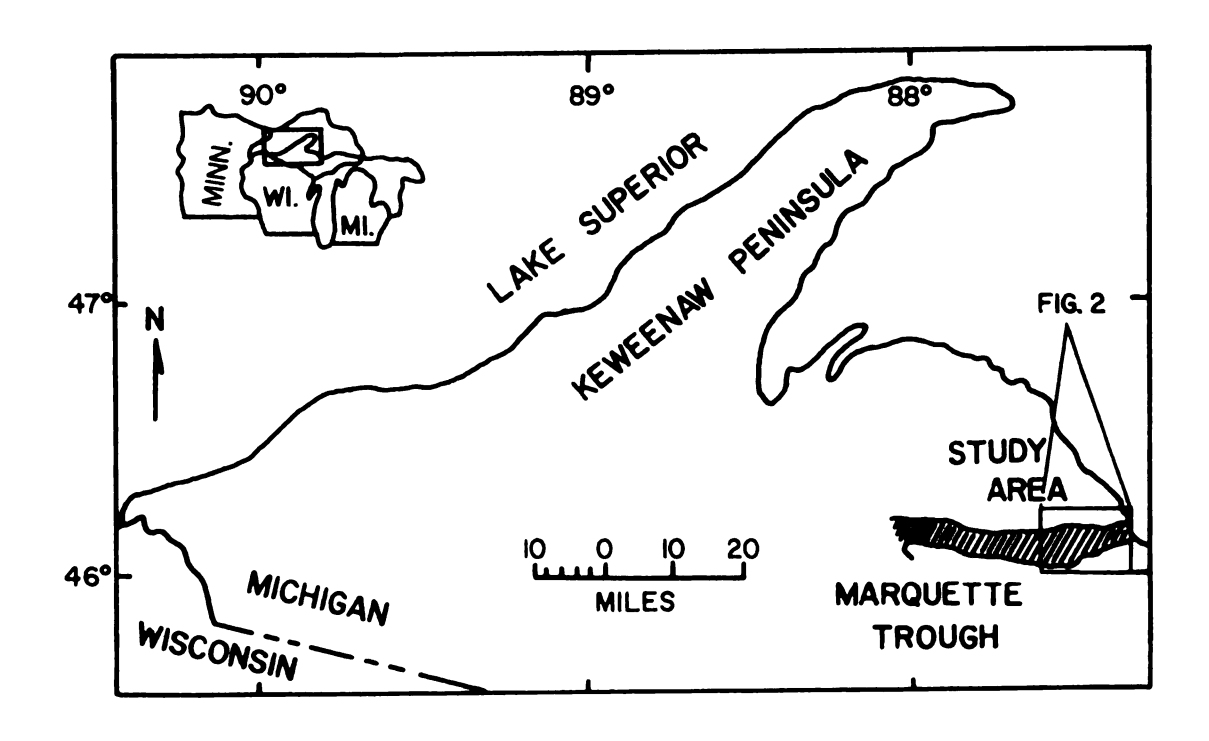


FIGURE |

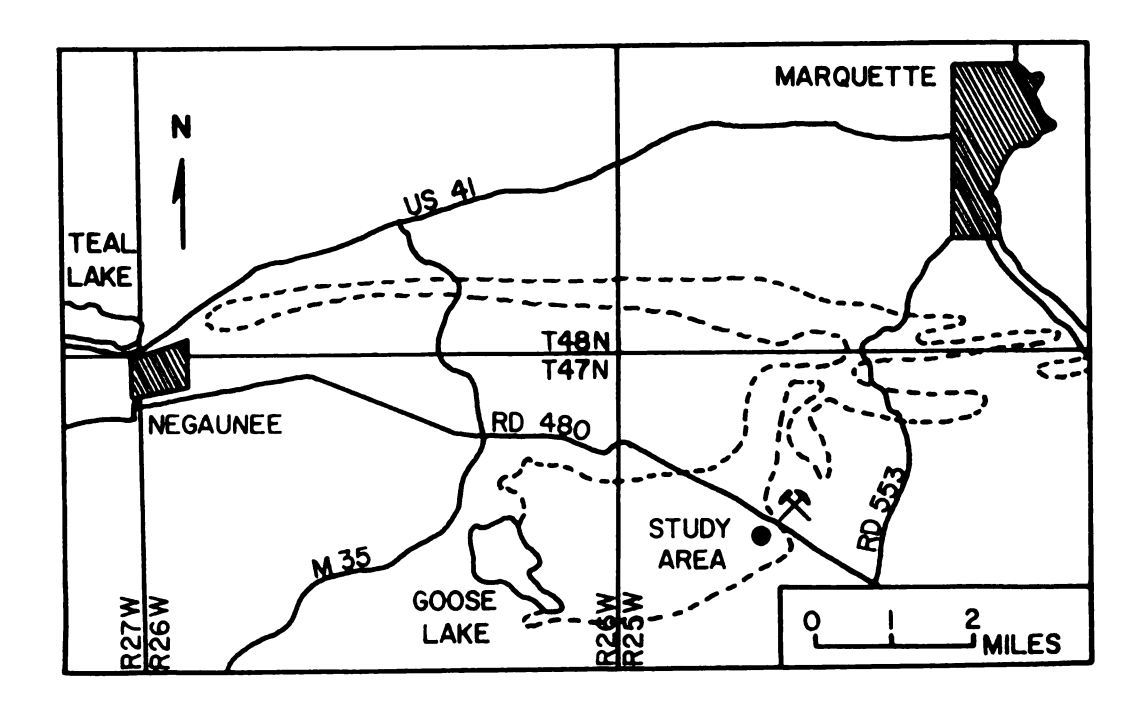


FIGURE 2



Figure 3. Photograph of flat-lying argillite containing reduction spots. Note long axes subparallel to bedding.

Figure 4. Photograph of folded slate containing reduction spots. Note long axes at a steep angle to bedding.



Figure 3



Figure 4

Reduction spot finite strains from both domains were obtained independently of the orientation of any material lines or planes with the following objectives in mind: 1) to constrain the predeformational distribution of the reduction spots from the strain state in the flat-lying layer; 2) to test the parallelism between the XY-plane of the reduction spots and the slaty cleavage; 3) to simulate the strain history by treating the different finite strain states as increments of the same progressive deformation; and 4) to integrate the results into a model for the tectonic evolution of the Marquette Trough.

Massive quartzite beds are intercalated with the argillites at the study locality. Based on a method described by Holst (1982), a semi-quantitative, two-dimensional measure of strain was obtained from the quartzites by analysis of the quartz grain shape fabric. This method was employed to test the usefulness of detrital grain shapes as strain indicators and to compare the style of deformation of the detrital grains to that of the reduction spots.

GEOLOGIC SETTING

Regional

The study area lies at the southern margin of the eastern Marquette Trough which is situated along the south edge of the Canadian Shield (Figure 1). Gair et al. (1968) mapped the region following an extensive geologic report by Van Hise et al. (1897). The Marquette Trough is a fault-bounded, east-west trending synclinorium of deformed, Middle Precambrian (Proterozoic-X) metasediments belonging to the Marquette Range Supergroup (stratigraphic nomenclature from Cannon et al., 1970). According to Sims et al. (1980), the Marquette Trough forms part of the "Great Lakes Tectonic Zone", inferred to be the suture between two Archaean crustal segments and the site of reactivation of tectonism during the Proterozoic.

The rocks investigated belong to the Kona Formation of the Chocolay Group and the lithologies have been described by Gair et al. (1968) and Taylor (1972). Taylor (1972) devised a stratigraphic sequence for the Kona Formation and proposed a model for the environments of deposition of the different lithologies. Larue et al. (1980) and Larue (1981) have proposed a depositional model within a tectonic framework for the rocks of the Chocolay Group as a whole.

Deformation and metamorphism in the Marquette Trough is attributed to the Penokean Orogeny (Cannon, 1973), which occurred approximately 1.85-1.95 b.y. ago (Van Schmus, 1976). Cannon (1973) interpreted the style of deformation as indicative of an extensional environment, and proposed that vertical tectonics best explain the folding present in the Marquette synclinorium. This model involves the deposition of the Marquette Supergroup on a peneplaned

Archaean basement and deformation of the sediments by regional gravity sliding. This produced gentle folds which were subsequently passively draped into the Marquette Trough by vertical motion along basement faults. Klasner (1974) revised the model proposing 3-4 stages of deformation in order to explain the fold patterns.

More recently, Cambray (1978) presented a plate tectonic model in which the Marquette Range Supergroup sediments were deposited in a structural trough formed on a rifted continental margin and subsequently folded in a compressional (collision-type) event which closed the Marquette Trough during the Penokean Orogeny. The compressional aspect of the deformation is strongly supported by the results of a regional finite strain study based on reduction spots in slates of the Kona Formation (Westjohn, 1978). Westjohn supported shortening of at least 45% in a north-south direction (i.e., normal to the margins of the Marquette Trough) by a flattening style of deformation.

Local

The study area is an abandoned quarry located south of Co. Rd. 480, 2.8 km west of the intersection with Co. Rd. 553 and less than 1 km north of the inferred contact between the Kona Formation and the underlying Archaean gneiss basement (Marquette County, Sands Quadrangle, R25W, T47N, NW%, NE%, Sec. 17; Figure 2, this study; Plate 2, Gair et al., 1968).

The thickness of Kona Formation exposed at the quarry is about 32 m. From the base upward, the lithologies and their approximate thicknesses are: massive pink-gray quartzite (5 m), red quartzitic dolomite (4.5 m), massive chert beds consisting of light breccia fragments in a deeply stained hematite matrix (3.5 m), tan-pink dolomite with cherty laminations and intercalations of laminated siltstone and silty mudstone (14 m), and at the top, dolomite with large, conical algal structures up to 1 m in diameter (5 m). Several beds of dark

gray-brown argillite are intercalated throughout the lower and middle sections with typical thicknesses of 0.3 m. The argillites contain the reduction spots used in this study. Following Taylor's (1972) stratigraphic nomenclature for the Kona Formation, the exposed section corresponds to the Big Cusp Algal Dolomite Member.

Figure 5 is a pace-and-compass map of the quarry showing the variation in bedding dips and orientations of structural features (i.e., joints, faults, dikes). Small-scale cross-laminations and algal structures demonstrate that the strata are not overturned. The large-scale structure is a broad, gentle syncline plunging about 15° to the southeast. Paralleling the apparent hinge of the fold is a shear zone ranging in width from 6-10 m. Bedding dips of 20° or more are exclusively limited to the north limb of the fold and to layers within this shear zone.

A north-northeast trending normal fault is exposed at the southeast corner of the quarry and an apparent throw of 5 m can be demonstrated by the relative displacement of marker beds. The major structural feature of the essentially flat-lying layers along the southern face of the quarry is a prominent, nearly vertical joint set cutting the "basal" quartzite. Many joints are filled with quartz up to 1 cm in width and display a constant attitude throughout the quarry in both flat-lying and tilted layers.

Along the western wall, several 3-8 m long and steeply dipping fault surfaces cut across bedding. The surfaces are clearly limited in length and terminate at layer boundaries. Slight vertical displacements can be observed across them in some cases. Others may be folded at the termination together with the adjacent layers. The folding of layers is limited to 1-2 m to either side of the fault surfaces.

Figure 5. Pace-and-compass map of study area.

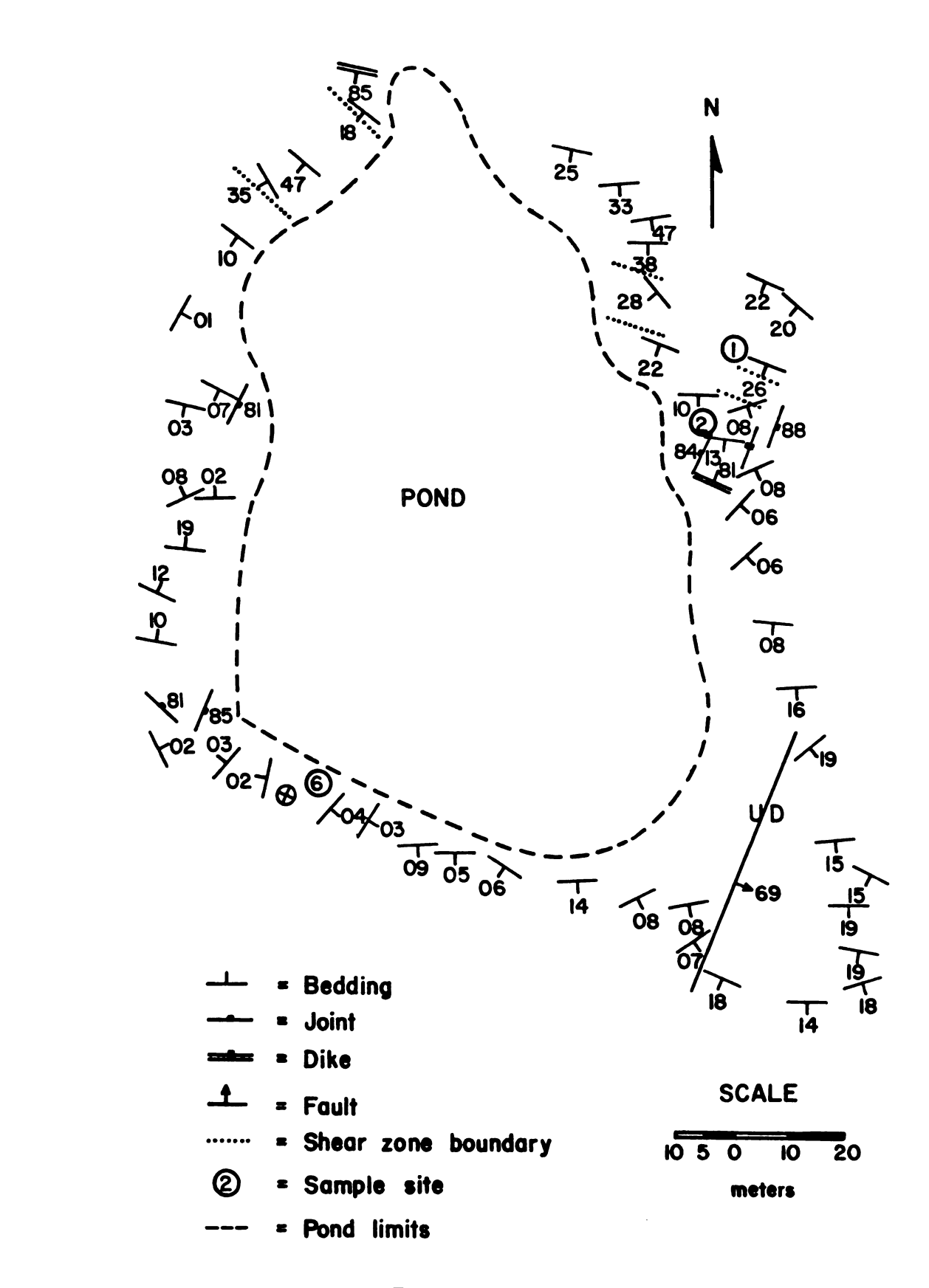
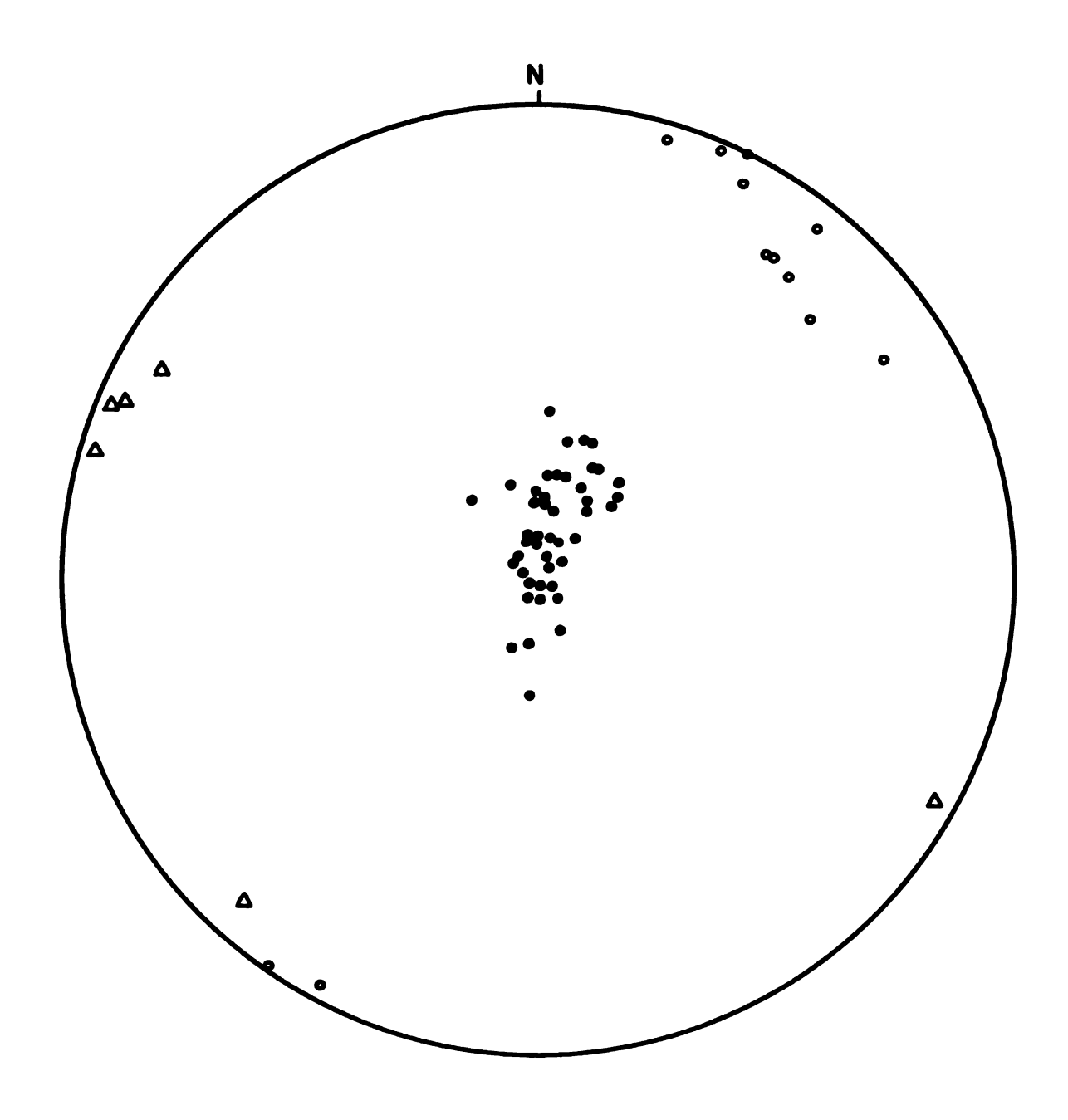


FIGURE 5

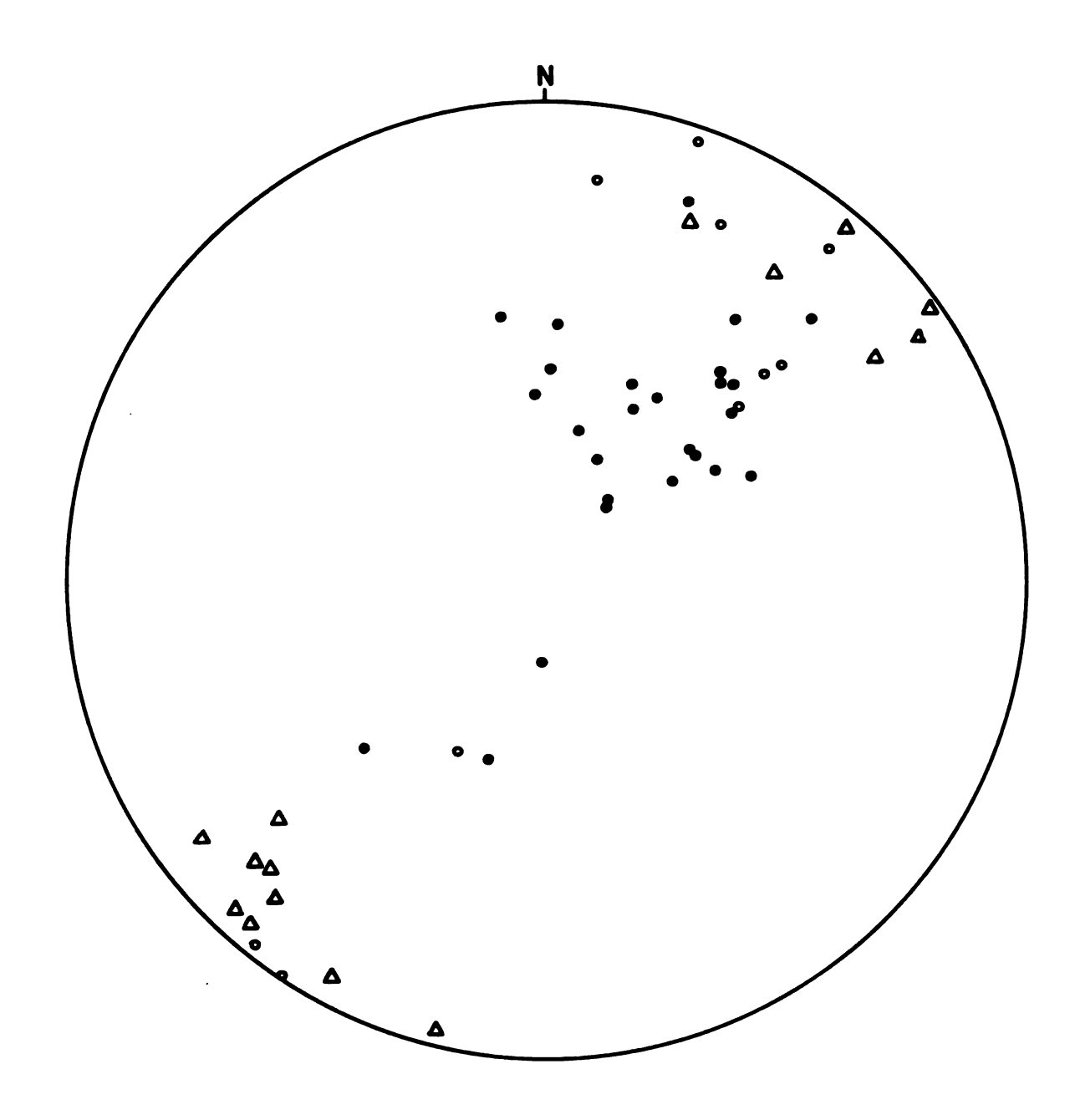
The shear zone boundaries along the northern edge of the quarry appear to be similar to the fault surfaces described along the western wall of the quarry in orientation, size and in the effect on the adjacent rocks. The "basal" quartzite bed is truncated at the southern boundary of the shear zone and a northside downward displacement of at least 4 m is inferred from the stratigraphic relationships. The strain intensity is highly variable within the zone. Blocks with gently dipping beds bounded by discrete fault surfaces alternate with zones of tight, upright similar-style folds. The limbs of these folds attain very steep dips and appear to be sheared by the faults. The argillites within the zone are strongly foliated and reduction spots reflect the "ductile" strain adjustments near the fault surfaces. The massive dolomite within the shear zone is highly fractured and in places displays a spaced, anastomosing foliation. The strike of the discrete fault surfaces within the shear zone and along the western face of the quarry are consistent with the northwest-southeast trend of the large-scale fold. The reader is referred to Figures 6 and 7 which are equal-area stereonet plots of poles to bedding, spaced cleavage, joints and fault surfaces.

The presence of reduction spots in the argillite beds and the variation in bedding dips within the quarry, provide an excellent opportunity for the evaluation of these strain markers in deformed and flat-lying rocks. The flat-lying rocks in particular, have the potential to provide insight into the initial distribution of the reduction spots.



- = BEDDING
- = SPACED CLEAVAGE
- Δ = JOINTS

FIGURE 6 STEREONET PLOT OF POLES TO BEDDING,
SPACED CLEAVAGE AND JOINTS (HIGH-STRAIN
ZONES EXCLUDED).



- = BEDDING
- = SPACED CLEAVAGE
- △ = FAULTS

FIGURE 7 STEREONET PLOT OF POLES TO BEDDING, SPACED CLEAVAGE AND FAULTS (HIGH-STRAIN ZONES).

DESCRIPTION OF SAMPLES

Sample Sites

Flat-lying argillites and quartzites were sampled at the base of the quarry along the southern wall (labelled #6 on Figure 5). At this site, the rocks display no signs of deformation other than the joints in the quartzite. Slightly tilted samples of quartzite were obtained just south of the shear zone (#2, Figure 5) and folded argillite was sampled from a bed just north of the shear zone (#1, Figure 5). The flat-lying and tilted quartzite samples are from the same layer. The thicknesses of the sampled argillites are comparable, about 0.3 m, though they are not the same layer. Slates from within the shear zone were not sampled because of the apparent inhomogeneous strain distribution within a volume of rock needed for a given sample.

At sample site #1, the dip of the folded argillite layer increases from 20 to 36° within 4 m. The layer thins and is intensely sheared at the northern boundary of the shear zone. The contacts with the underlying and overlying massive quartzitic dolomite are highly irregular and in places faulted.

Cleavages

The folded argillite (hereafter termed slate) contains two cleavages, a slaty cleavage and a spaced cleavage. The spaced cleavage (1-2 cm spacing) is curviplanar, discontinuous and stands out because of a lighter green colour of the phyllosilicates. Slight shear displacements can be observed across a few of the surfaces. These represent real displacement in the sense that the displacement cannot be accounted for by strain involving domainal volume change (Williams, 1976a). The spaced cleavage displays a strong lineation interpreted as arising

from the preferred orientation of grains parallel to the elongation direction in that plane. The lineation plunges 31-37° southeast. The spaced cleavage appears to continue for a distance of 20-30 cm with some refraction into the massive dolomite.

The slaty cleavage is weakly developed and hence seldom apparent at the outcrop (Figure 8). The strike is similar to that of the spaced cleavage but the dip angle is shallower by 5 or more degrees. Parallel to the slaty cleavage there is a preferred orientation of the grains plunging 75-85° northwest (Figure 9). It is clear, however, that a variety of other orientations are represented. In thinsection the two cleavages appear to crosscut each other in a simple manner, i.e., without any apparent deflection or rotation.

Petrographic Descriptions

Argillite and Slate. Contains 35-40% quartz, 50-55% sericite, 5-8% opaques, 3-6% chlorite and minor microcline. Sericite is mostly clay-size with a few large (.05-.08 mm) muscovite grains and aspect ratios of 1:5 and 1:12. Eight percent of the quartz is present as angular, subequant grains of very fine sand size, distributed as thin silty laminae or sinous, nearly vertical channels (possibly mudcracks). The remainder of the quartz is present as silt- and clay-size particles with irregular shapes and embayed boundaries. Opaque minerals are present as angular, equant grains. Chlorite forms tabular grains with aspect ratios of 3:1-5:1. In places the argilite contains abundant replacement nodules after evaporite minerals now consisting of chert, dolomite and chloritoid.

In the flat-lying argillites there is a slight preferred orientation of the micas in the bedding plane, trending east-southeast and southeast as shown qualitatively on a rose diagram of the orientation of the long axes of grains in that plane (Figure 10). Perpendicular to bedding, the large muscovite grains are subhorizontal in orientation.

Figure 8. Optical micrograph of slate perpendicular to slaty cleavage and bedding (crossed polars). Cleavage trace dips to bottom right, bedding trace to bottom left. Scale = 1 cm:29 microns.

Figure 9. Optical micrograph of slate approximately parallel to slaty cleavage (crossed polars). Preferred orientation dips to bottom left, bedding trace to bottom right. Scale = 1 cm:15 microns.

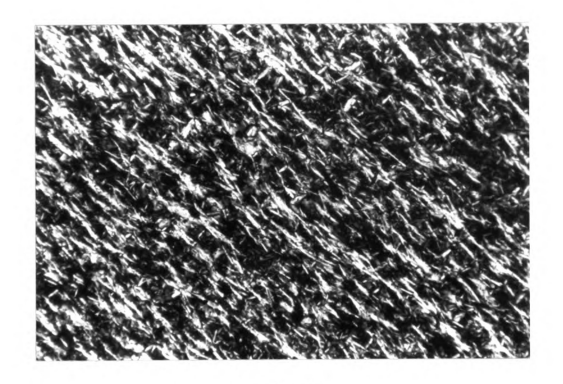


Figure 8

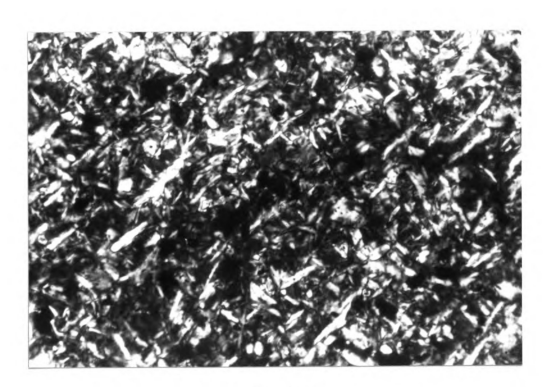
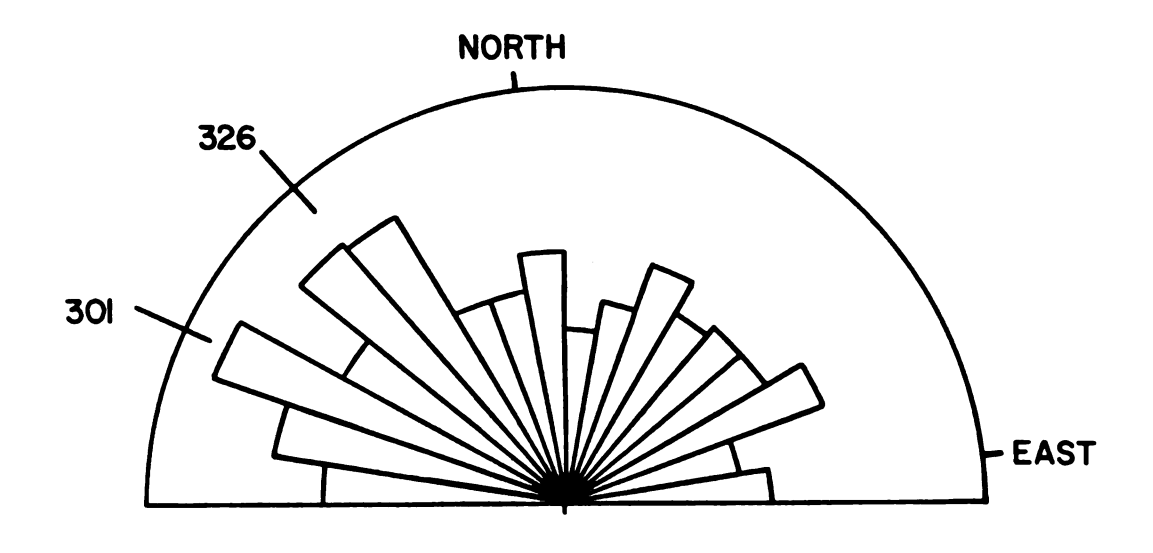


Figure 9



NUM. OF GRAINS = 200 INTERVAL = 10°

FIGURE 10 ROSE DIAGRAM OF THE ORIENTATION OF LONG AXES OF GRAINS IN THE BEDDING (HORIZONTAL) IN FLAT-LYING ARGILLITE.

In the slate, the preferred orientation of micas defines the slaty cleavage.

Other orientations are represented and, in particular, the large muscovite grains remain subparallel to bedding.

Reduction Spots. Except for a conspicuous lack of opaque minerals, the reduction spots are mineralogically indistinguishable from the surrounding matrix (Figure 11). Some of the "spots" are faulted and their shapes strongly modified by cross-cutting veins or spaced cleavage. A few spots contain roughly concentric, circular to elliptical, distinctly coloured zones separated from each other by sharp boundaries. Others are surrounded by a pink zone with diffuse outer boundaries in contact with the matrix. Variations in the sharpness and regularity of the presumed initial spot-matrix boundaries do not appear to be affected by the presence or absence of these zonations. Optically, the morphology of the "spot" boundaries appears to be unchanged between flat-lying and folded argillites. The zonations are interpreted as arising from diffusion-and reaction-controlled processes during late diagenesis and metamorphism.

Quartzite. Contains 85% quartz, 10% dolomite and 5% microcline, albite, muscovite and opaque minerals. Quartz (with straight and wavy extinction) and feldspar are present as detrital grains (.04-.65 mm) in an irregularly distributed dolomicrite matrix and matrix seams of micas. "Dust rings" preserve the rounded, subequant shapes of the detrital quartz surrounded by overgrowths in optical continuity with the host grain. In areas of extensive overgrowths several polygonal subgrains have formed with straight extinction. The boundaries between many neighboring quartz grains (and overgrowths of adjacent grains) are embayed and in some cases marked by strings of small, slightly misoriented subgrains (Figure 12). Quartz grain-dolomite boundaries are fairly even while quartz overgrowth-dolomite boundaries are cuspate.

Figure 11. Optical micrograph of reduction spot boundary in slate (uncrossed polars). Reduction spot at bottom. Scale = 1 cm:150 microns.

Figure 12. Optical micrograph of deformed quartzite. Note partially corroded "dust rings", embayed boundaries and polygonized subgrains. Scale = 1 cm:65 microns.

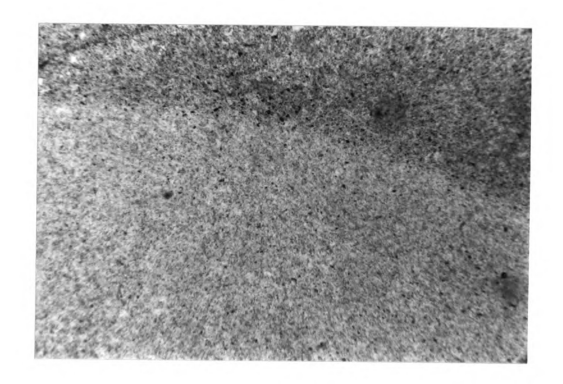


Figure 11

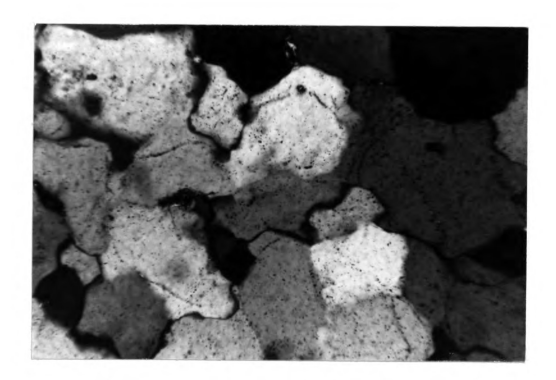


Figure 12

Qualitatively, there is no preferred orientation to the quartz overgrowths and no apparent textural difference between the flat-lying and tilted quartzite.

ANALYSIS: ASSUMPTIONS AND METHODOLOGY

Finite Strain from the Quartz Grain Shape Fabric in Quartzites

A two-dimensional measure of strain was obtained from the quartz grain shapes in the quartzite based on the method described by Holst (1982). Holst measured the distribution of particle shapes (pebbles, clasts, colites and pisolites) on variously oriented planes in undeformed rocks. After simulating superimposed homogeneous strains, he concluded that by using an error function accurate strains can be obtained assuming the initial orientation to be random. The error increases when the two-dimensional section studied is at a high angle to bedding.

Oriented thin sections of the quartzite were photographed and a sampling grid superimposed on the image; the spacing of the grid was determined from the largest observed grain diameter. The following parameters were measured:

D1 = length of long axis

D2 = length of short axis

 ϕ = angle of long axis with respect to an arbitrary reference line

For irregularly-shaped grains the longest dimension of the grain was taken as the major axis of the "ellipse" and the longest dimension perpendicular to it as the minor axis. One hundred grains were measured for each sample. The following parameters were calculated:

$$\varepsilon = \frac{1}{2} \ln \left(\frac{D1}{D2} \right)$$

 $\theta = 2\phi$

and these were used to construct polar plots of the distributions (Elliott, 1970). For each point with coordinates (ϵ , θ) the Cartesian coordinates were calculated:

 $X = \varepsilon \sin \theta$

 $Y = \varepsilon \cos \theta$

The point given by $(\overline{X}, \overline{Y})$ was taken as the center point of the distribution where:

$$\overline{X} = \sum_{i=1}^{n} (X_i)/n$$

$$\overline{Y} = \sum_{i=1}^{n} (Y_i)/n$$

The orientation of this point is given by:

$$\overline{\theta} = \tan^{-1}(\overline{X}/\overline{Y})$$

and the strain ratio for an ellipse located at that point by:

$$\bar{S} = e^{2\bar{\epsilon}}$$

where

$$\bar{\epsilon} = (\bar{X}^2 + \bar{Y}^2)^{\frac{1}{2}}$$

is the magnitude of the vector to the center point.

Finite Strain from Reduction Spots

The method employed for the determination of strain from reduction spots requires that the following assumptions be made: homogeneity of strain at the scale of the "spots", negligible volume changes during deformation and initial sphericity or a random distribution; these assumptions will be discussed briefly.

The size of measured reduction spots ranges from 0.3-2.5 cm. At this scale, inhomogeneity of strain caused by mineral and grain anisotropies may be neglected. Furthermore, since the ductility contrast is expected to be minimal, homogeneity with respect to the surrounding matrix may be assumed. Inhomogeneous strain may be expected near layer boundaries and chert-dolomite nodules; large variations of axial ratios and orientations were observed near the latter. Reduction spots less than 5 cm from such features were excluded from the analysis.

Ramsay et al. (1973) discuss the geometric effects of volume change and Wood (1973) evaluates the errors that might arise from various volume losses.

While there is no apparent way of quantifying volume changes during deformation, calculations show that changes of 15% or less can be neglected, but greater gains or losses in volume would introduce significant errors in the strain values measured (Wood, 1973). The similar morphology of the reduction spot boundaries found in the flat-lying and folded argillites is an argument lending support to the assumption that volume changes were minimal.

The assumption of initial sphericity is difficult to evaluate. Aside from the geometric evidence discussed later in this paper, some support for a predeformational spherical form was found by Miller et al. (1955). The authors found "spots" of both irregular and spherical shapes in undeformed sandstones. A similar shape distribution has been observed by this author in sandstones of the Jacobsville Formation near Marquette, Michigan. The critical aspect of the problem is the extent to which an initial preferred orientation of grains controls the diffusional process believed to be responsible for the "spots".

Experimental investigations and studies concerning the initial preferred orientation in unconsolidated argillaceous sediments indicate that the microstructure is complex and variable (Rieke et al., 1974). During deposition, dispersed clays will tend to settle as subhorizontal platlets while flocculated clays will form differently oriented domains of clay aggregates (O'Brien, 1970). Flocculation is enhanced by electrolytic sea water and/or high concentrations of clays in suspension. The effects of dispersion and flocculation control the degree of preferred orientation as well as the development of bedding plane fissility during compaction (O'Brien, 1970). The flat-lying argillites of this study do not display any bedding fissility and therefore an initial microstructure with little or no preferred orientation may be assumed in this case.

There is no evidence regarding the precise timing of formation of reduction spots. It is proposed that if the reduction spots in the studied argillites formed

shortly after deposition, they will adopt a spherical shape by the diffusion of components through a quasi-random grain microstructure. Subsequent compaction produced flattened reduction spots with circular sections in the bedding plane.

For the determination of finite strain from reduction spots, two-dimensional data from three mutually orthogonal planes is combined to calculate the strain ellipsoid (p. 142-147, Ramsay, 1967). The revised form of the Fortran program STRDET (Oertel, 1978; Miller et al., 1979) is used for the calculations. In order to derive mean plane tensors with errors, the method requires that the values of the tensor components, referred to a common coordinate system, have a normal distribution. Histograms constructed by the computer program allow qualitative evaluation of this assumption, and in this study (though not always Gaussian) none of the plane tensor distributions were strongly skewed.

Individual samples of argillite were cut into three mutually orthogonal sets of oriented slabs and photographic prints of enlarged spots were obtained. The long and short axes of the reduction spots were drawn directly on the photographs and visually checked to fit the symmetry principles for ellipses. The lengths of the orthogonal axes were measured (D1 and D2) and the pitch of the long axis. The size of the sample obtained for a given plane ranged from 51 to 83 reduction spots. The maximum number of measurable reduction spots for a given sample varied from 153 to 234. The reader is referred to the Appendix for the analysis of errors involved in the strain determination from both the quartz grains and the reduction spots.

Models of Progressive Deformation Based on Reduction Spot Finite Strain States

The field evidence strongly supports the argument that the reduction spots at the locality record compactional strain prior to the tectonic strains responsible for the folding. It is extremely unlikely that the flat-lying rocks

have been tilted and then returned to a horizontal position without the accompanying effects on fabric as observed in the folded layers. Thus, the shape and orientation changes undergone by the reduction spots have been modelled in two general stages: a) flattening of an initial sphere by gravitational compaction, and b) superimposed tectonic strains.

Sedimentary compaction was modelled by axially symmetric shortening (X = Y > Z) parallel to the vertical Z-axis. The length of the horizontal X=Y axes was calculated, $X = (Volume/Z)^{\frac{1}{2}}$. The assumption of negligible volume change is misleading in this case since most of the compactional strain is volumetric, i.e., resulting from the water expelled in response to the applied stress (Rieke et al., 1974). According to Skempton (1970) the consolidation of argillaceous sediments may involve volumetric strains of 30-70% considering a minimum overburden thickness of 100 m.

The modelling of the tectonic strains is based on the assumption that the flat-lying and folded reduction spot samples represent different increments of finite strain within a single, progressive deformation. This assumption is justified because: 1) there is no evidence that the large-scale fold structure developed during more than one distinct tectonic event, and 2) the folded samples were obtained from outside the shear zone. By comparison, deformation within the shear zone is clearly localized and the rocks have a different strain history than those outside the shear zone.

Two types of homogeneous deformation were modelled to simulate tectonic strains: pure shear and simple shear. Pure shear was modelled using the bedding plane unstraining technique described by Ramsay (1967), p. 130-132. This method is based on the changes in the angles of the intersections of the bedding plane with the principal planes of the ellipsoid. The principal elongations were adjusted by subtracting "undeformed" from "deformed" lengths as illustrated in Figure 13:

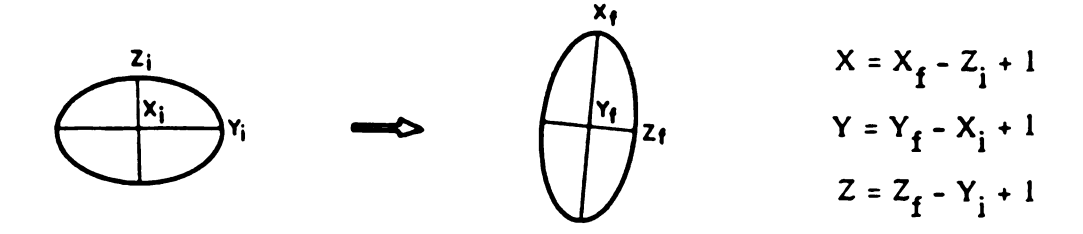


Figure 13. Method of adjusting principal elongations for pure shear.

Simple shear was modelled by calculating the rotation of a material line relative to the shear direction (Ramsay, 1967). For a given increment the attitude of the shear plane and shear direction is maintained constant. The principal elongations were adjusted by subtracting "undeformed" from "deformed" lengths as shown in Figure 14:

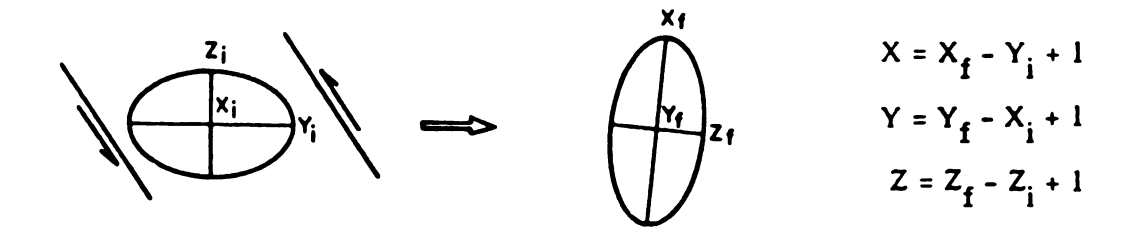


Figure 14. Method of adjusting principal elongations for simple shear.

The elongation of the intersection line is calculated (numbers in parentheses to the right are those of Ramsay's, 1967 equations):

$$\lambda' = \lambda_1'^2 + \lambda_2' m'^2 + \lambda_3' n'^2$$
 (4-7)

where $\lambda' = 1/\lambda$ and l', m', n' are the direction cosines in the deformed state.

Shear strain is calculated:

$$\gamma'^{2} = (\lambda_{1}' - \lambda_{2}')^{2} l'^{2} m'^{2} + (\lambda_{2}' - \lambda_{3}')^{2} m'^{2} n'^{2} + (\lambda_{3}' - \lambda_{1}')^{2} n'^{2} l'^{2}$$
(4-17)

where $\gamma' = \gamma/\lambda$

The amount of rotation of the intersection line is then calculated:

$$\cot \alpha = \cot \alpha' - \gamma \tag{3-71}$$

where α and α' are the angles between the line and the shear direction in the "undeformed" and "deformed" states, respectively.

Strictly simultaneous superimposition of simple shear and pure shear is not possible. Finite increments of either strain type may be applied sequentially and the size of the increments depends on the different states represented by the samples. Since the samples of this study only represent three different strain states, the increments are rather large, i.e., 5% shortening in pure shear.

In the modelling of simple shear, errors are introduced when it is attempted to constrain the maximum and minimum strain axes of both "undeformed" and "deformed" states to lie on a single plane. The errors are considered to be negligible with the exception of modelling involving sample LQ-6-12.

RESULTS AND DISCUSSION

Finite Strains from the Quartz Grain Shape Fabric in Quartzites

Figures 15 and 16 are polar plots for the flat-lying and slightly tilted quartzites, respectively. The calculated strain parameters are presented in Table 1. Mean values for these parameters from the study of undeformed rocks by Holst (1982) are included in Table 1 for comparison. The graphs and the calculated parameters are interpreted as indicative of a random distribution of quartz grains. The low values of $\bar{\epsilon}$ and values for \bar{S} close to one are within the range characteristic of random distributions in undeformed rocks studied by Holst (1982). The difference in these values for the flat-lying and tilted quartzite is ascribed to the difference in attitude of the sample plane with respect to bedding.

The method employed is not sensitive enough to measure the strains undergone by the quartzites; that is, the quartz grain shapes in the quartzites do not record the strains calculated from reduction spots in comparable argillites.

Embayed boundaries, small subgrains at the boundaries and polygonized subgrains may be interpreted as arising from the motion and interaction of dislocations (dislocation glide and creep) and grain-boundary diffusion, i.e., cobble creep (Nicolas et al., 1976; White, 1976). These mechanisms do not appear to have been pervasive enough to extensively alter the original grain shape fabric and to produce a preferred orientation. A significant amount of strain may have been accommodated by grain-boundary sliding without a change of shape of the grains ("particulate flow" of Borradaille, 1981). Borradaille (1981) proposed that such mode of intergranular strain may be expected during the initial deformation under low-grade metamorphic conditions of rocks with

Table 1. Strain parameters from the quartz grain shape fabric in the quartzites.

		Sample					
Sample Number	Bedding Attitude*	Plane Attitude*	Measured Grains	ıω	+ ιω	S	+ \S
LQ-6-2	Horizontal	191/69	100	.09 ± .03	40. ± 80.	1.20 ± .08	1.17 ± .08
LQ-2-1	11/183	10/195	100	.01 ± .03	.02 ± .02	1.02 ± .08	1.04 ± .03

* = Dip angle/direction.

† = Mean values for planes of similar attitude with respect to bedding, from Holst (1982).

 $\bar{\epsilon}$ = Vector to center point. \bar{S} = Strain ratio at center point.

Figure 15. Polar plot of quartz grain shape fabric in flat-lying quartzite (LQ-6-2). Black triangle is center point of distribution.

Figure 16. Polar plot of quartz grain shape fabric in tilted quartzite (LQ-2-1). Black triangle is center point of distribution.

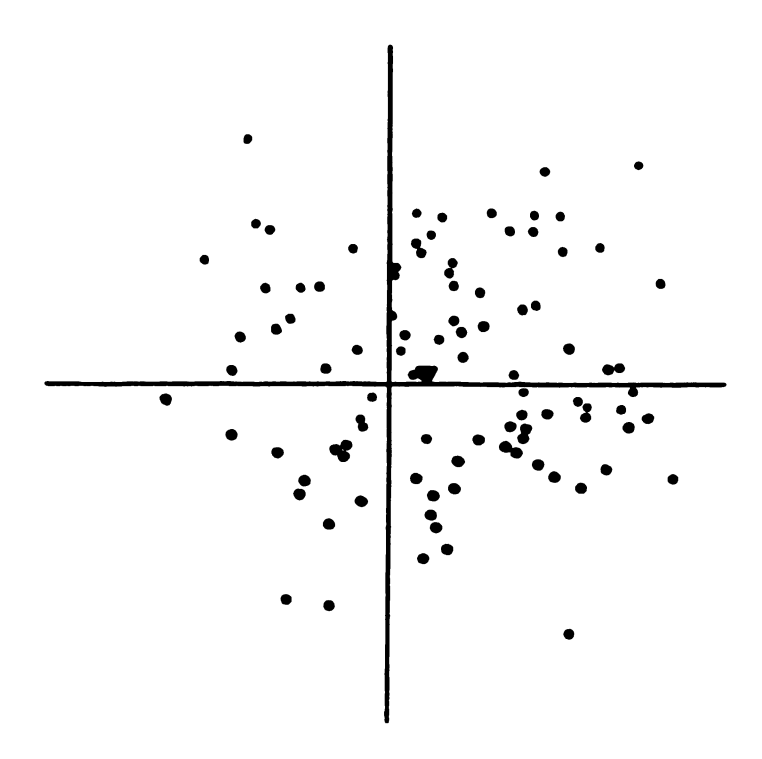


FIGURE 15

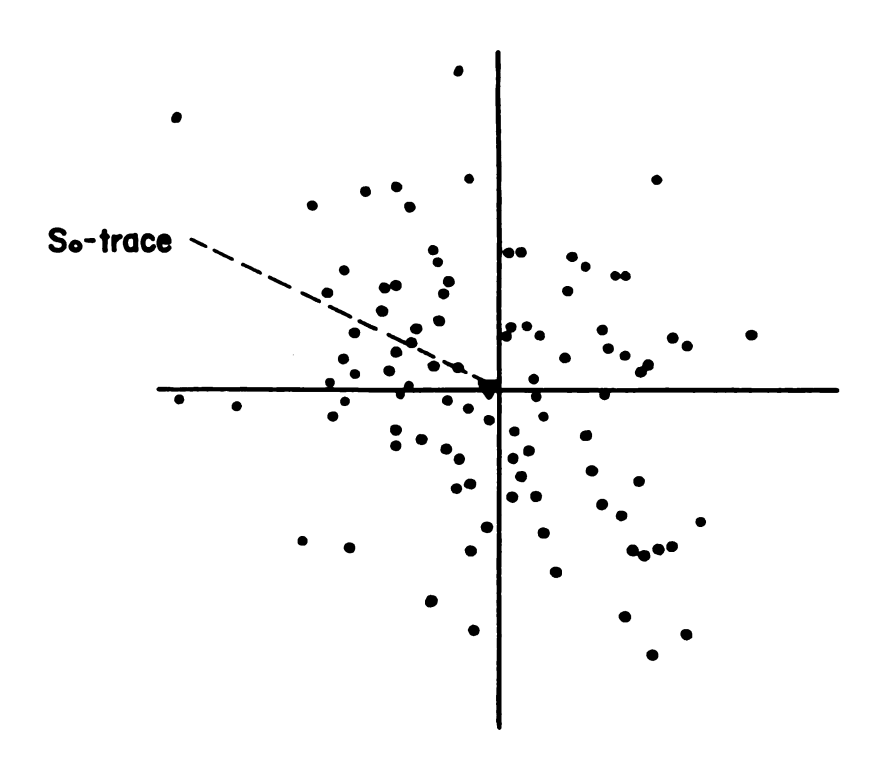


FIGURE 16

relatively high fluid pressures. To test this hypothesis it would be necessary to obtain a measure of the strain accommodated by intragranular deformation mechanisms and evaluate the degree of interdependence of inter- and intragranular deformation mechanisms.

The north-northeast trending joint set in the quartzite layers is interpreted as resulting from horizontal extension in a west-northwest direction and this is consistent with the initial deformation history recorded by the reduction spots. The extensive quartz filling of the joints implies that significant mass transfer has occurred and this may account for some of the additional reduction spot strain.

Finite Strains from Reduction Spots

In Table 2 the magnitudes of the principal strains for all samples are listed. The strain intensity factor ε_s is proportional to the distortion of the strain ellipsoid and ν is Lode's parameter describing the shape of the strain ellipsoid. Figure 17 is a stereonet plot of the principal strain axes for the two flat-lying reduction spot samples. Separate stereonet plots are presented for each of the two folded samples, showing in addition the orientation of bedding, slaty cleavage, spaced cleavage and associated lineations (Figures 18 and 19).

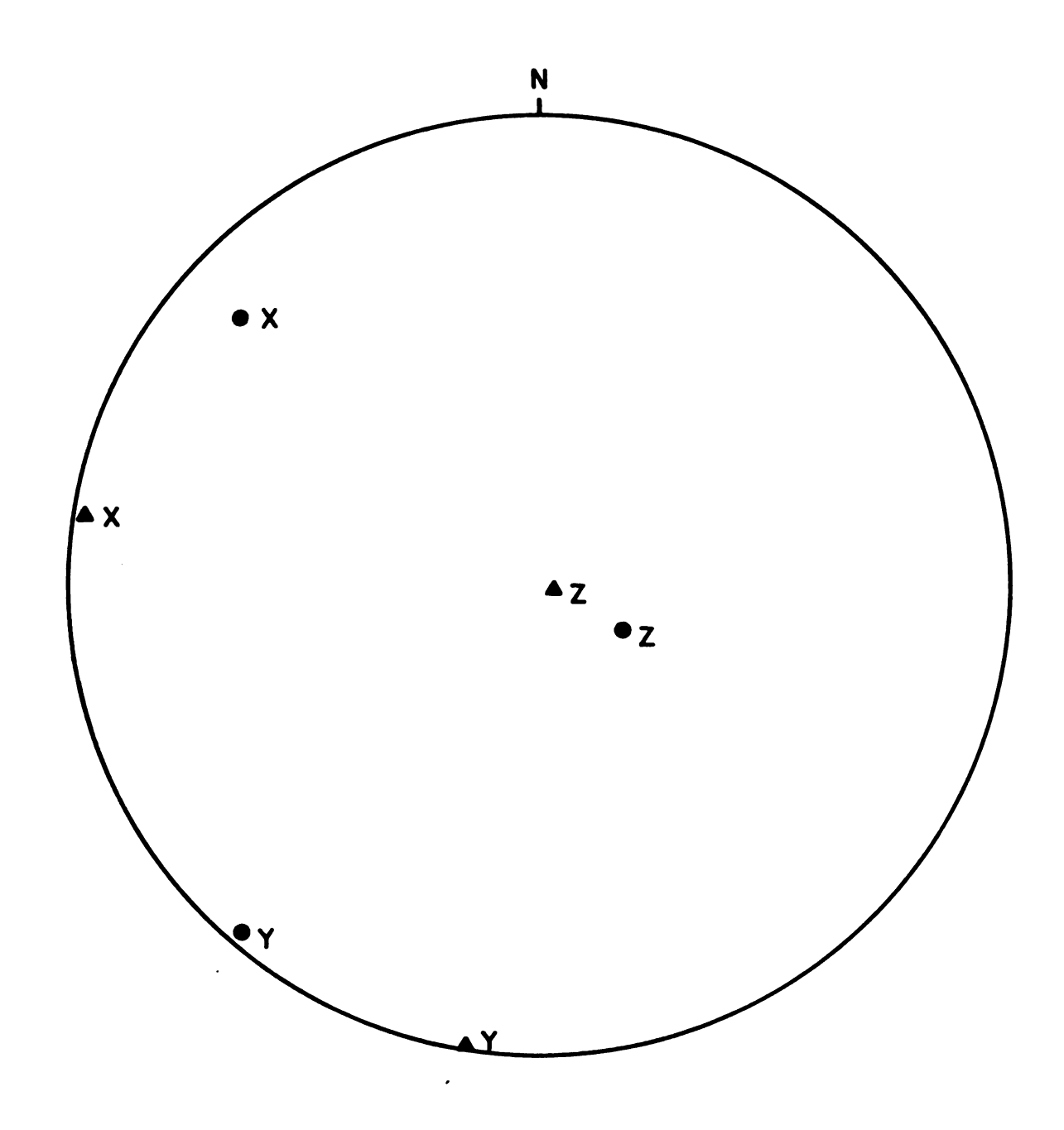
Figure 20 is a plot of the mean axes ratio of individual data planes versus the range in measured orientations of the long axis (D1). It illustrates: 1) the considerable scatter of orientations of D1, 14° being the minimum, 2) an apparent exponential increase of the range with decreasing ratio, and 3) the apparent lack of interdependence between the range of orientations of D1 and the dip angle of the data plane. The inverse proportionality between the ratio and the range of D1 orientations is interpreted as resulting primarily from the orientation of the data plane with respect to the circular sections

Table 2. Strain parameters from reduction spots in argillite and slate.

Sample	Bedding	† ;	+;	+		
Number	Attitude*	×	Ā	7	S	2
LQ-6-12	Horizontal	1.4119 ± .030	1.0085 ± .015	.6984 ± .008	.502	.036
LQ-6-2	Horizontal	1.3031 ± .036	.9857 ± .019	.7785 ± .016	.365	084
LQ-1-9	16/176	1.1835 ± .047	1.1558 ± .029	.7311 ± .036	.384	.902
10-1-6	25/177	1.3380 ± .033	1.1014 ± .024	4£0. ± 9879.	464 °	.427

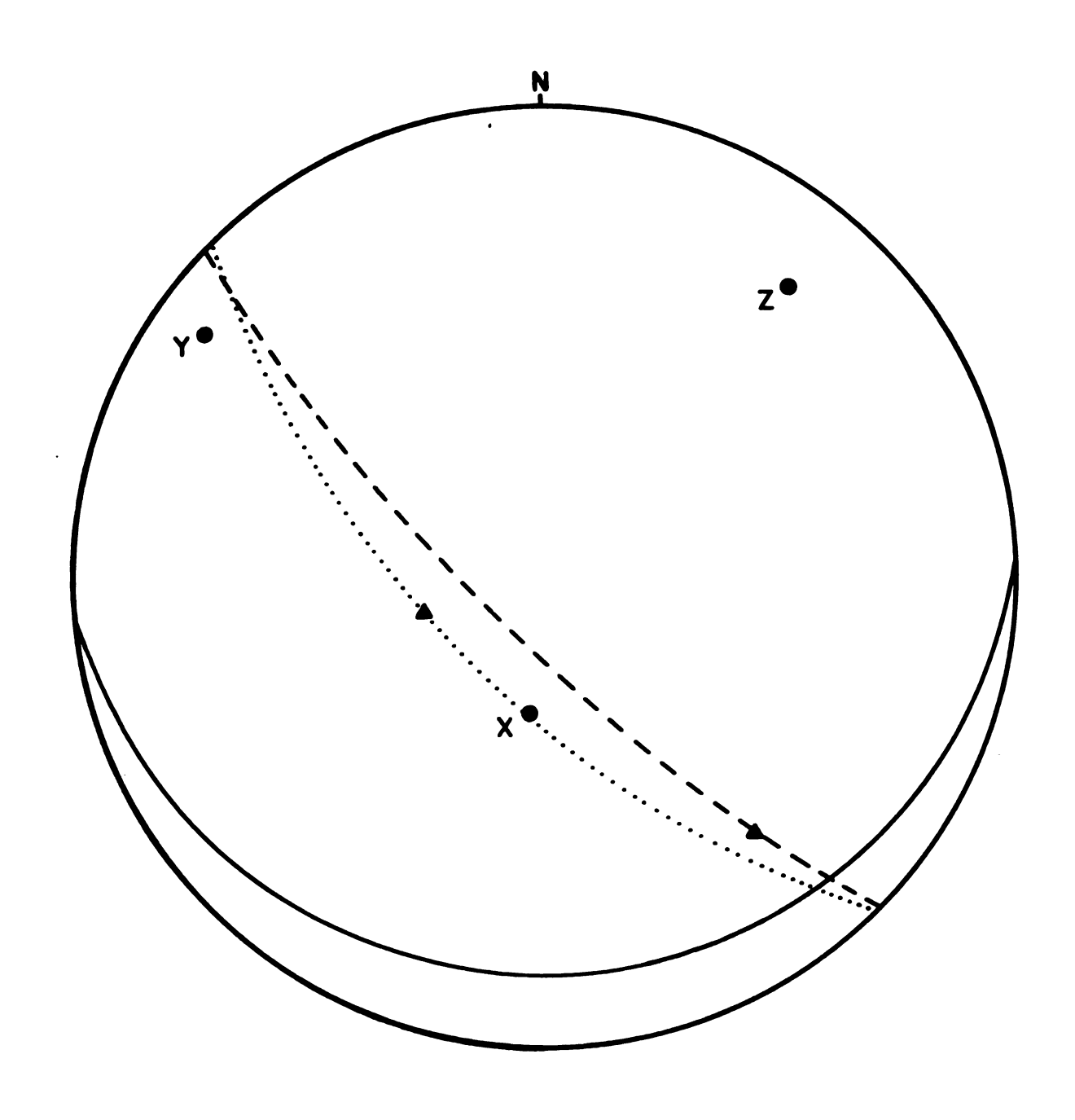
* Bedding attitude as dip angle/direction.

⁺ X, Y, Z are (e₁ + 1), (e₂ + 1), (e₃ + 1), respectively $\varepsilon_{S} = 1/3\{(\varepsilon_{1} - \varepsilon_{2})^{2} + (\varepsilon_{2} - \varepsilon_{3})^{2} + (\varepsilon_{3} - \varepsilon_{1})^{2}\}^{\frac{1}{2}}$ $v = \{(2\varepsilon_{2} - \varepsilon_{3})/(\varepsilon_{1} - \varepsilon_{3})\} - 1$ where $\varepsilon_{i} = \ln(\varepsilon_{i} + 1)$



● = SAMPLE LQ-6-2 ▲ = SAMPLE LQ-6-12

FIGURE 17 STEREONET PLOT OF PRINCIPAL STRAIN AXES FOR FLAT-LYING ARGILLITES.



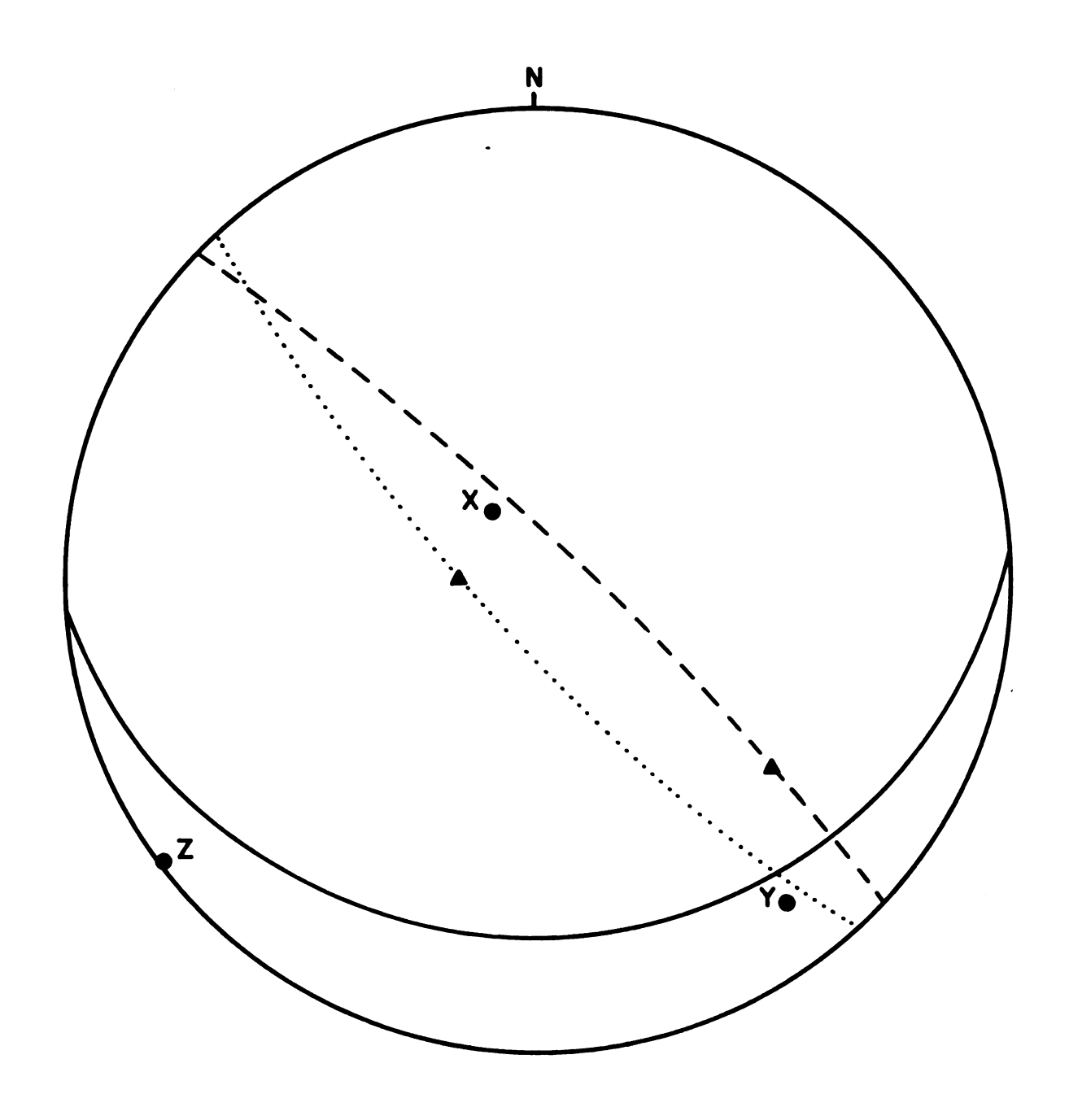
- = BEDDING

--- = SPACED CLEAVAGE

..... = SLATY CLEAVAGE

▲ = LINEATIONS

FIGURE 18 STEREONET PLOT OF PRINCIPAL STRAIN AXES, BEDDING, CLEAVAGES AND LINEATIONS FOR FOLDED SLATE (LQ-1-9).



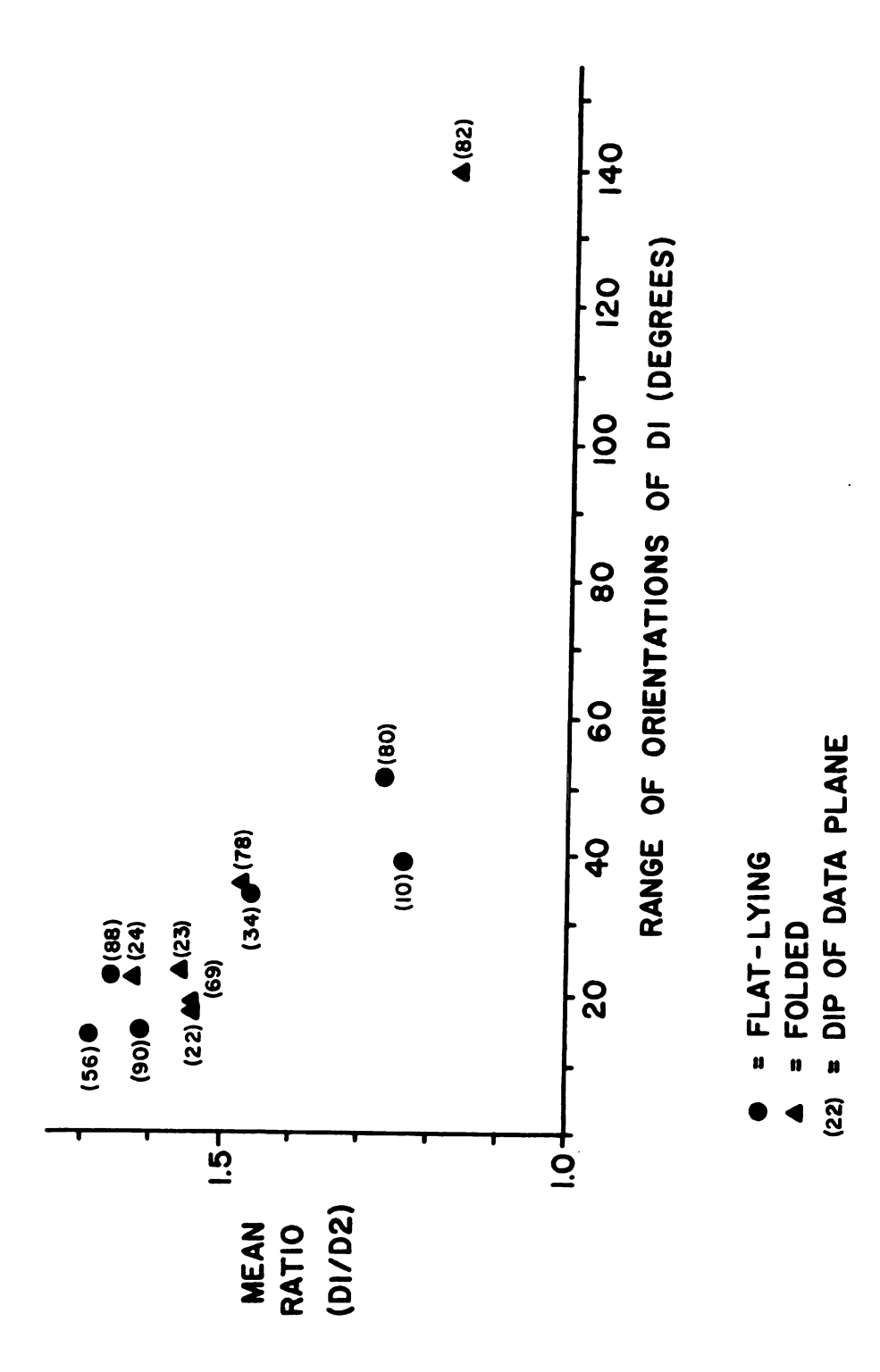
- = BEDDING

--- = SPACED CLEAVAGE

..... = SLATY CLEAVAGE

▲ = LINEATIONS

FIGURE 19 STEREONET PLOT OF PRINCIPAL STRAIN AXES, BEDDING, CLEAVAGES AND LINEATIONS FOR FOLDED SLATE (LQ-1-6).



DATA PLANES VERSUS THE RANGE IN ORIENTATIONS PLOT OF MEAN AXES RATIO OF REDUCTION SPOT OF THE LONG AXIS (DI). FIGURE 20

(near which the range would be large) of a given ellipsoid, and only to a minor degree from observational error.

The folded samples show different orientations of principal axes but in both cases the XY-plane roughly parallels the trend of the cleavages. The slaty cleavage is parallel to the XY-plane of the strain ellipsoid derived from reduction spots considering the directional error of 5° for the strain axes. The difference in bedding dip for the two folded samples (9°) is reflected consistently by the strain magnitudes of the principal axes, Table 2. This confirms the validity of the reduction spots as strain indicators and suggests that the analytical method is sensitive enough to record minor strain differences. In addition, the consistency of the strain variation justifies treating the two folded samples as different finite strain states.

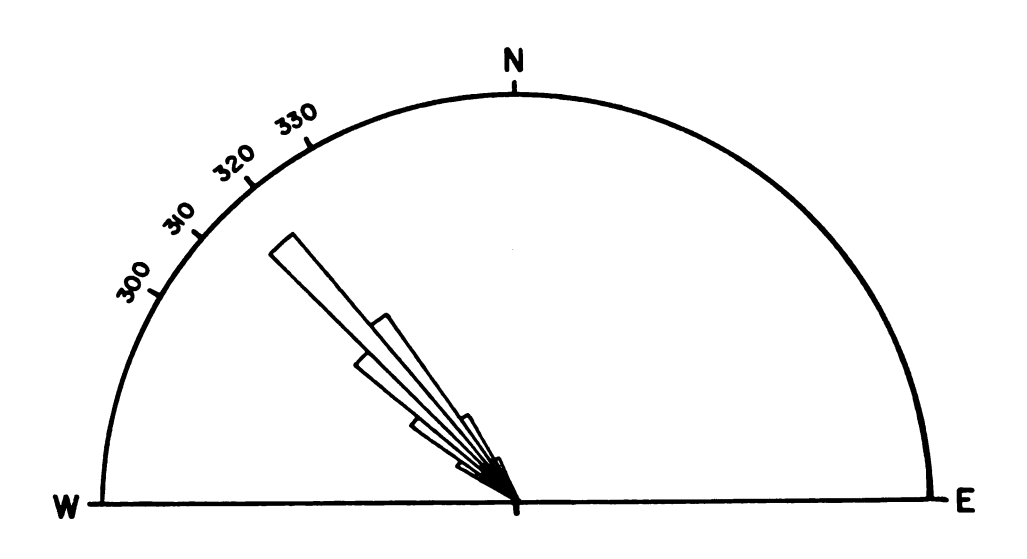
The results for the flat-lying samples are more difficult to interpret. The XY-plane for one of the samples (LQ-6-2) is parallel to the XY-plane in the slates, but deviates from this trend by about 30° for the other sample, LQ-6-12 (Figure 17). In both cases, the horizontal bedding is not parallel to a circular section of the strain ellipsoid (Table 2, Figure 17). In light of these results, the assumptions of initial sphericity and absence of a sedimentary preferred orientation need to be evaluated again.

Three alternative hypothesis may be considered: the reduction spots represent 1) tectonically undeformed, compactional strain with a variable preferred orientation in the bedding plane, 2) tectonic strains superimposed on a compactional fabric with unknown preferred orientation(s) in the bedding, and 3) tectonic strains superimposed on a compactional fabric without a preferred orientation in the bedding. Hypothesis (3) is preferred from the arguments presented earlier but aspects relevant to the evaluation of all three models will be discussed in the following paragraphs.

If the flat-lying are assumed to be tectonically undeformed they record a maximum compaction of 23-31%. This is distinctly below the range reported for argillaceous sediments (Skempton, 1970; Rieke et al., 1974) and hypothesis (1) can be rejected.

During incremental, irrotational strain, lines initially oblique to the XY-plane of strain (e.g., a preferred orientation in the bedding plane) will tend to reorient themselves parallel to the XY-plane or the X-axis under flattening and constrictional strains, respectively (Ramsay, 1967). It would seem fortuitous if the X-direction of sample LQ-6-2 represents a sedimentary preferred orientation. It is possible that both flat-lying samples together show the scatter expected from the dispersion of lines between the initial preferred orientation and the X-axis of strain. The preferred orientation of grains in the bedding plane does not support this hypothesis (Figure 10). Figure 10 shows two maxima (301 and 326) at approximately equal angular distance from the trend of the XY-plane (about 312). To further test this hypothesis, the direction of long axes of reduction spots was measured on the bedding plane of an additional flat-lying sample; the results are displayed in the rose diagram of Figure 21. The diagram shows a single maximum trending northwest (about 317), paralleling the strike of the XY-plane in the slates and the XZ-plane of sample LQ-6-2. These results strongly support model (3), i.e., the reduction spots in the flat-lying argillites record tectonic strains superimposed on a compactional fabric without a sedimentary preferred orientation in the bedding plane.

The difference in orientation between the two flat-lying samples may be ascribed to a slight deviation from the "ideal" compaction history and/or the heterogeneous nature of the initial incremental strains.



NUM. OF SPOTS = 109 INTERVAL = 5°

FIGURE 21 ROSE DIAGRAM OF THE ORIENTATION OF LONG AXES OF REDUCTION SPOTS PARALLEL TO BEDDING IN FLAT-LYING ARGILLITE (LQ-6-IO).

Model of Progressive Deformation Based on Reduction Spots

The modelled deformation of the reduction spots can be divided into four stages: 1) compaction of initially spherical reduction spots, 2) layer-parallel flattening up to the finite strain state represented by the flat-lying argillites, 3) and 4) two consecutive increments of combined pure shear and simple shear, from the flat-lying argillites to the folded slate (LQ-1-9) and from LQ-1-9 to LQ-1-6, respectively. Neither pure shear or simple shear alone can account for the observed strain magnitudes and orientations. Progressive intervals of pure shear were applied followed by simple shear. Sample LQ-6-12 cannot be modelled by simple shear with respect to the folded samples and was therefore excluded from the modelling of tectonic strains..

Several combinations of compaction and layer-parallel flattening appear possible. The shallow stretching lineation in the spaced cleavage is interpreted as indicating that the northwest direction was one of infinitesimal extension relative to the subvertical strain axis during the deformation path from the flatlying to the folded finite strain states. Infinitesimal shortening must have occurred along this direction during later strain increments. Therefore it is postulated that during the initial deformation increments (i.e., post-compaction and prior to significant folding) the northwest-horizontal strain axis was one of zero infinitesimal strains and/or infinitesimal extension. This allows the amount of compaction to be constrained by the finite strains in the flat-lying layer assuming that the vertical and northeast-horizontal strain axes were extension and shortening directions, respectively, during deformation. There is no evidence supporting more complex models, e.g., one involving additional changes in the sign of elongation in the northwest-horizontal direction during deformation.

<u>Compaction</u>. Sedimentary compaction was modelled in 5% intervals using the following criteria: 1) the resulting Z (vertical) axis should be shorter than that now found in the flat-lying argillite, and 2) the resulting X (horizontal-northwest) axis should be shorter or equal to that now found in the flat-lying layers. These parameters constrain the amount of compaction to 30-50%. For the sake of modelling 40% was chosen as an average resulting in an oblate ellipsoid with dimensions, X = Y = 1.291 and Z = 0.6. The calculated amount of compaction lies within the lower half of the geologically reasonable range reported by Skempton (1970) and Rieke et al. (1974).

Layer-parallel flattening. For the modelling of this increment the principal elongations of the "compaction" finite strain ellipsoid were subtracted from the corresponding strain axes in the sampled flat-lying layer. This results in layer-parallel flattening of 30% in a northeast-southwest direction. Such flattening as a prefolding stage is an agreement with theoretical and experimental studies regarding the folding of single-and multi-layers; about 31% (Hobbs et al., 1976), about 35% (Sherwin et al., 1968).

Flat-lying (LQ-6-2 to folded (LQ-1-9). The choice of a suitable shear plane and shear direction is the most critical aspect of this and the following increment of strain. To test the model of flexural folds (Ramsay, 1967), an attempt was made to model the deformation by shearing parallel to bedding. This does not yield satisfactory results: 1) The angle between the maximum elongation and the shear direction is 15° larger than that predicted by the model; 2) The elongations deviate by 15-17% from those predicted by the model; 3) Superimposed shortening perpendicular to the axial plane cannot produce the observed angular relationships between the strain axes and bedding; and 4) Additional shortening prior to layer-parallel shearing can be modelled but the

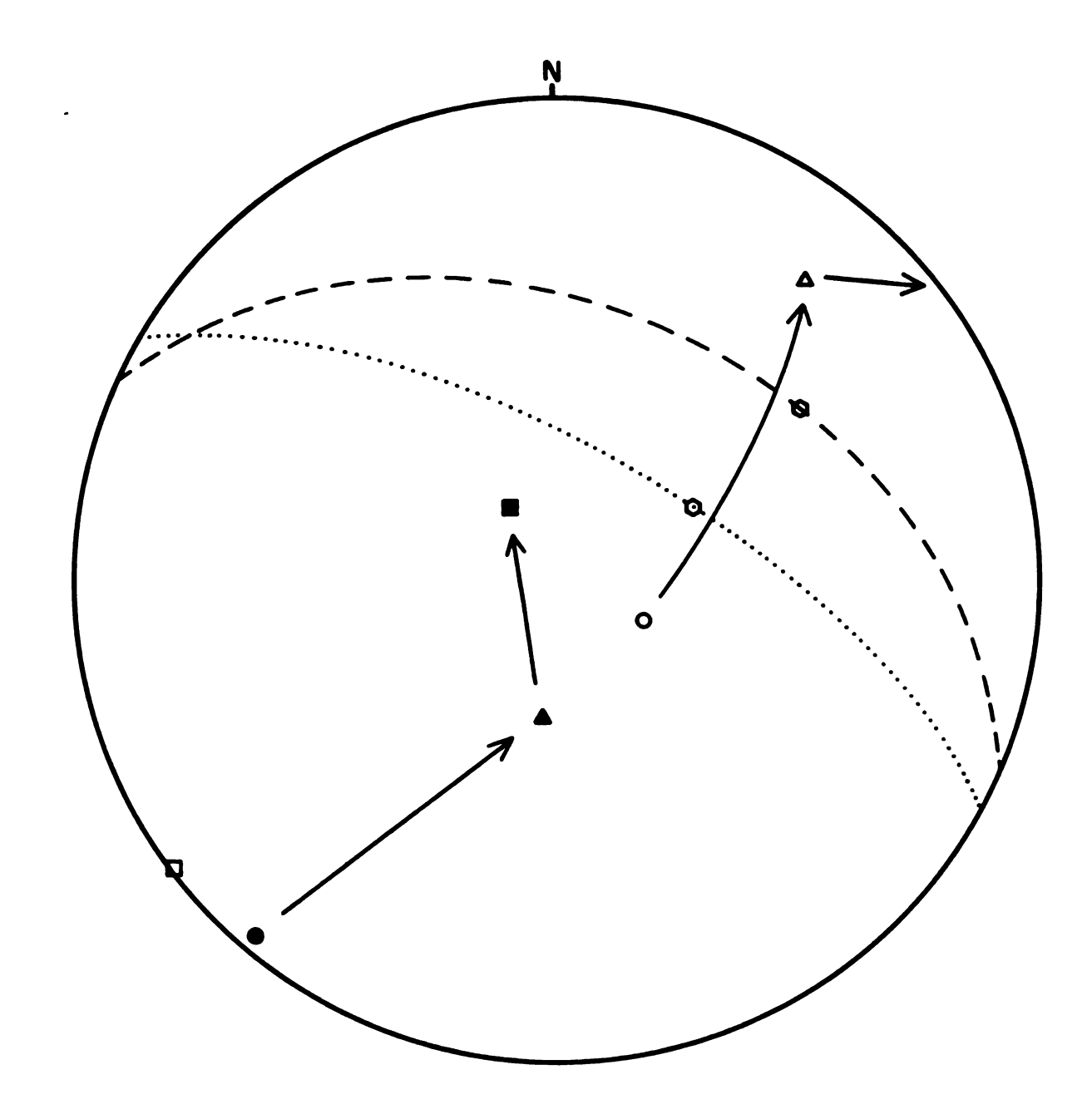
sense of the superimposed shear cannot account for the apparent rotation of the X-axis from sample LQ-1-9 to LQ-1-6.

As noted before, the contacts between the slate and the massive dolomite are highly irregular and crenulated and thus the boundaries themselves would not be likely slip planes. The development of several order buckle folds during compressive deformation of multilayers of contrasting competency has been modelled by Ramberg (1964). It is suggested that the slate-dolomite boundaries may display such "microbuckling".

The modelled shear planes and shear directions have to be oblique to bedding and a choice was made based on the following criteria: 1) the correct relative rotation of the finite strain axes; 2) the axes of maximum extension for the samples are all steep but dipping in different directions; this suggests that the maximum incremental stretch did not deviate significantly from the vertical axis throughout the deformation; 3) the presumed maximum incremental stretch is always at 45° to the shear direction, the subsequent finite maximum elongations making progressively smaller angles; 4) the shear plane and direction chosen for this increment of deformation should not be radically different from those which satisfy conditions 1) through 3) for the next increment of deformation (i.e., LQ-1-9 to LQ-1-6).

Based on these criteria the shear plane dips 43/024 and the shear direction 39/056 (Figure 22). The deformation modelled involves 10% pure shear shortening and simple shear ($\gamma = .30$). The model requires that the subhorizontal X-axis in the flat-lying argillite extend during the initial 5% pure shear increment. During the next increment it begins to shorten and extension occurs only in a subvertical direction.

The morphology of the folded slate-dolomite boundaries at the thin-section scale provides some support for the modelled shear plane and direction. The



- ---- SHEAR PLANE (LQ-6-2 TO LQ-1-9)
- ----- = SHEAR PLANE (LQ-1-9 TO LQ-1-6)
- ▲ = PROGRESSIVE LONG AXES ORIENTATION
- O △ □ = PROGRESSIVE SHORT AXES ORIENTATION

FIGURE 22 STEREONET PLOT OF MODELLED SHEAR PLANES AND DIRECTIONS.

crenulations are asymmetric with respect to the finite strain axes. The sense of rotation displayed is consistent with the proposed shear direction if we assume that the initial buckles developed as smooth, rounded folds. The sketch in Figure 23 illustrates the observed relationships:



Figure 23. Diagram illustrating the relationship between the modelled shear and microbuckles.

In theory, the shear planes may be infinitely close and need not be visible in naturally deformed rocks (Ramsay, 1967).

Folded (LQ-1-9 to LQ-1-6). Using the same criteria as described above the modelling requires a steepening of the shear plane, 68/030, and of the shear direction 64/064 (Figure 22). The increment of deformation involves 5% pure shear shortening and simple shear ($\gamma = .03$). There is no visible evidence supporting the steepening of the shear plane. Jaeger (1960) and Walsh et al. (1964) investigated theoretical and experimental aspects of shear failure in rocks containing a planar anisotropy. Although based on slightly different criteria, their conclusions were essentially the same: shear failure would occur on a single plane of fracture which lies between the plane of minimum shear strength and the nearer to it of the two conjugate directions possible on the Coulomb theory. The deviation rises to a maximum and then falls off as the angle between the planar anisotropy and the maximum compression direction approaches zero (Jaeger, 1960). Assuming that the subvertical cleavage

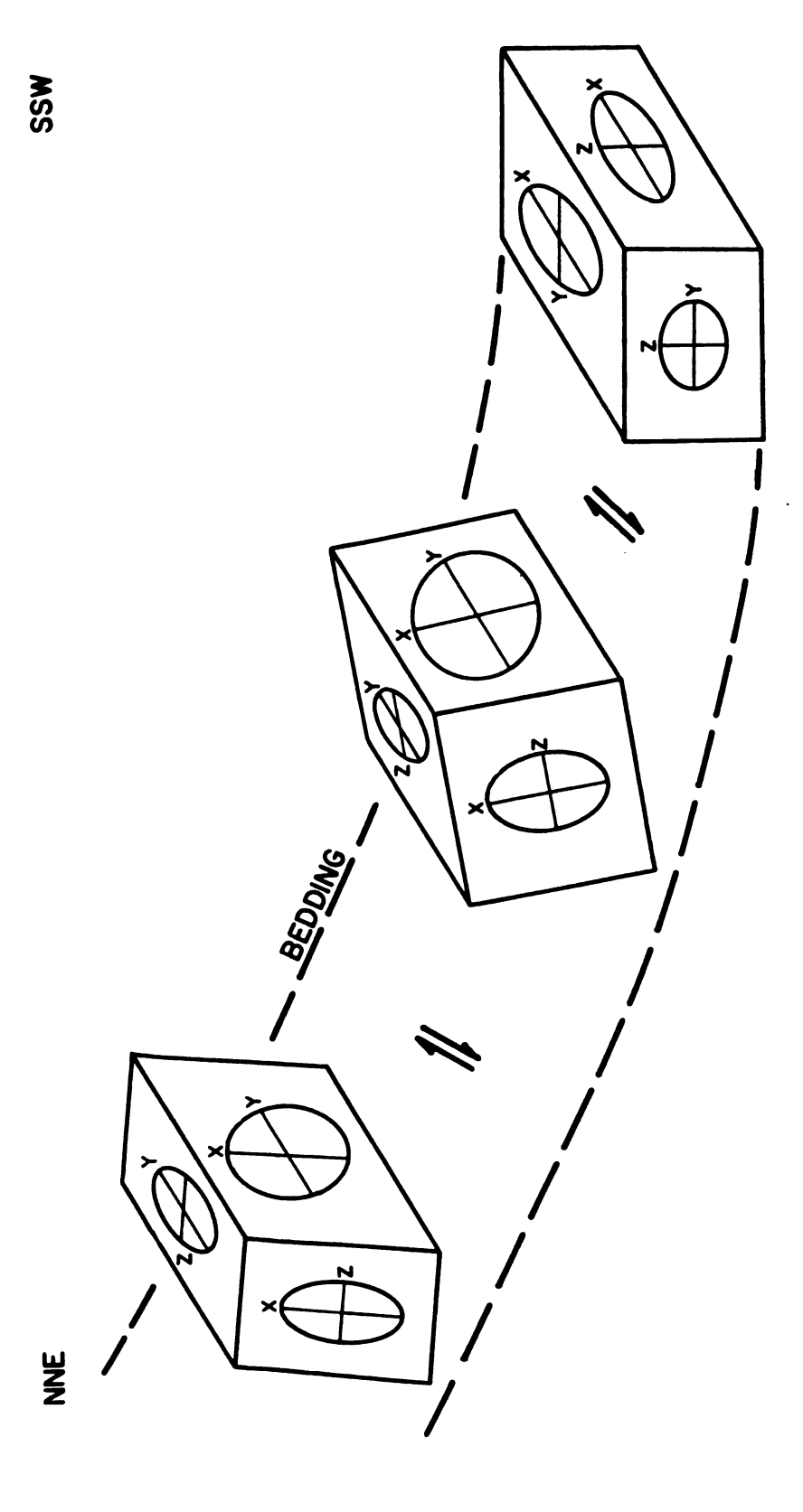
represents the planar anisotropy of least shear strength, the steepening of the shear plane is consistent with their model. Figure 24 is a block diagram schematically illustrating the progressive deformation of the reduction spots from the flat-lying to the folded layers.

Table 3 summarizes the results of the modelling of the progressive deformation in terms of the subhorizontal northeast and northwest strain axes and the subvertical axis. Figure 25 is a graph of the observed and implied finite strain states. It illustrates the progression from an oblate ellipsoid (X = Y > Z) to plane strain (X > Y = 1 > Z) and to pure constriction (X > Y = Z), back across the plane strain line to nearly pure flattening (X = Y > Z), and finally into the flattening field (X > Y > 1 > Z). A similar sequence has been documented by Graham (1978) on a much larger scale in Permian rocks of the Maritime Alpes.

Implications of the Model for Progressive Cleavage Development

The slates contain both a discrete, spaced cleavage and a pervasive slaty cleavage. The spaced cleavage displays a stretching lineation plunging 31-37° southeast and the preferred orientation in the slaty cleavage plunges 75-85° northwest (Figures 18 and 19). Within the model of deformation of this study, the spaced cleavage must have formed while the subhorizontal northwest strain axis was an extension direction relative to the subvertical axis. Furthermore, the change in dip direction (80° southwest to 84° northeast) and plunge of lineation (31 to 37° southeast) is consistent with progressive rotation during folding.

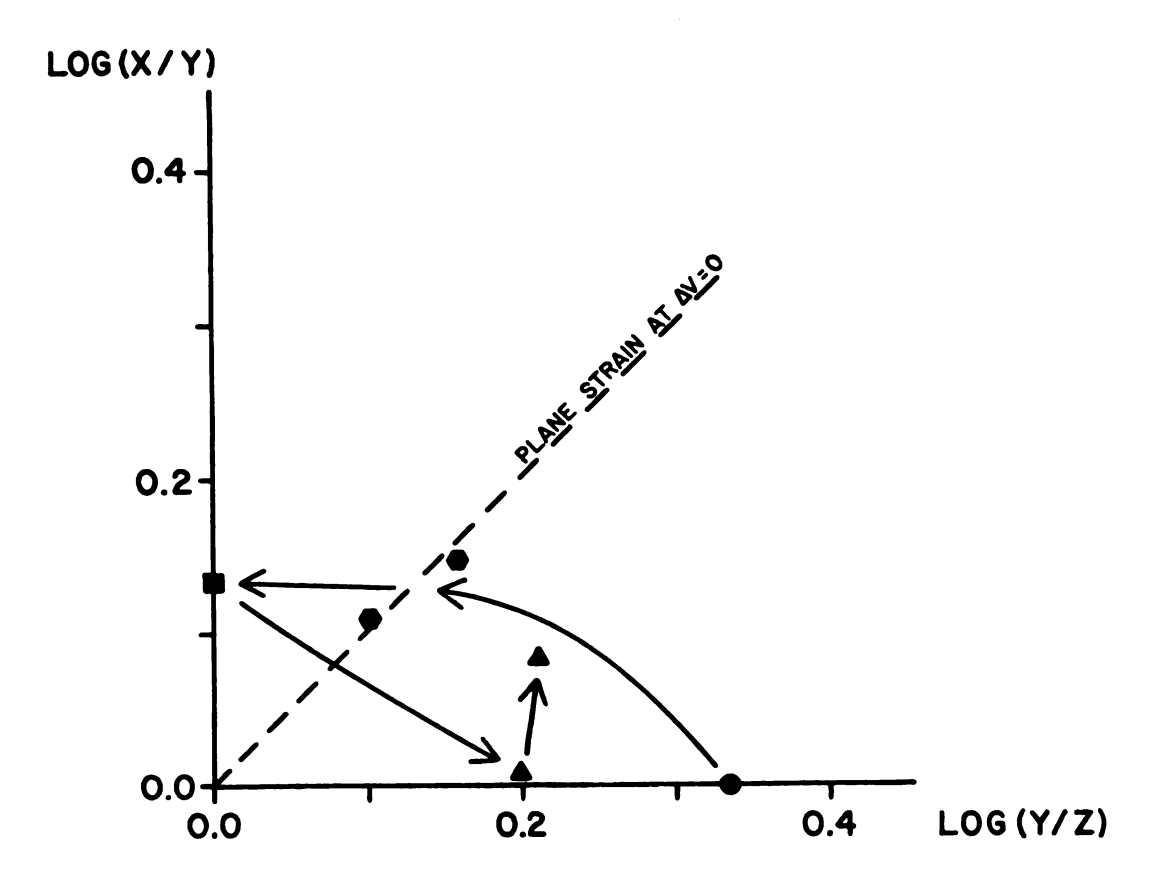
The steep lineation in the slaty cleavage implies that the latter must have started to develop during a later strain increment when the subhorizontal northwest strain axis ceased to be an extension direction. This interpretation is based on the assumption that the preferred orientation of grains in the slaty cleavage cannot adjust to the changing orientation of the elongation direction



SCHEMATIC DIAGRAM OF THE PROGRESSIVE DEFORMATION OF REDUCTION SPOTS FROM FLAT-LYING TO FOLDED LAYERS. FIGURE 24

Table 3. Strain components for the deformation increments modelled.

Doformation	Pure Shear Components			Shaar
Deformation Increment	NE(%)	NW(%)	V(%)	Shear Strain
Compacted to Flat-lying	-30	+1	+17	
Flat-lying to Folded LQ-1-9	-10	-2	+10	.30
Folded LQ-1-9 to Folded LQ-1-6	-6	-7	+15	.03
Total Pure shear Components	-46	-8	+42	



• = COMPACTED

• = FLAT-LYING

= INTERMEDIATE

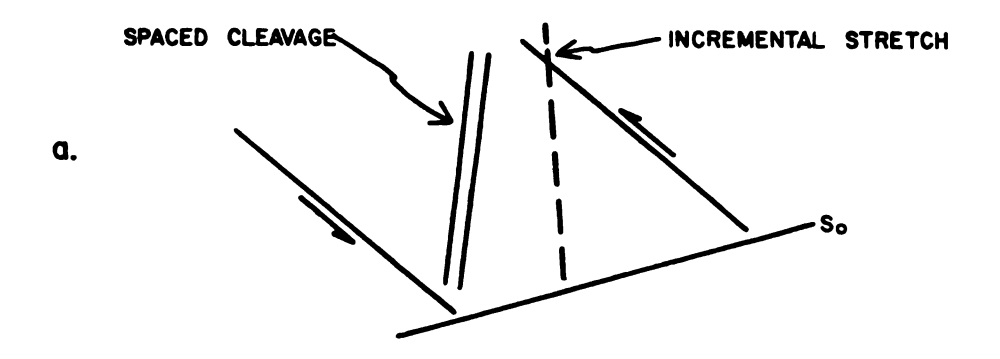
▲ = FOLDED

FIGURE 25 GRAPH OF MEASURED AND IMPLIED REDUCTION SPOT FINITE STRAIN STATES.

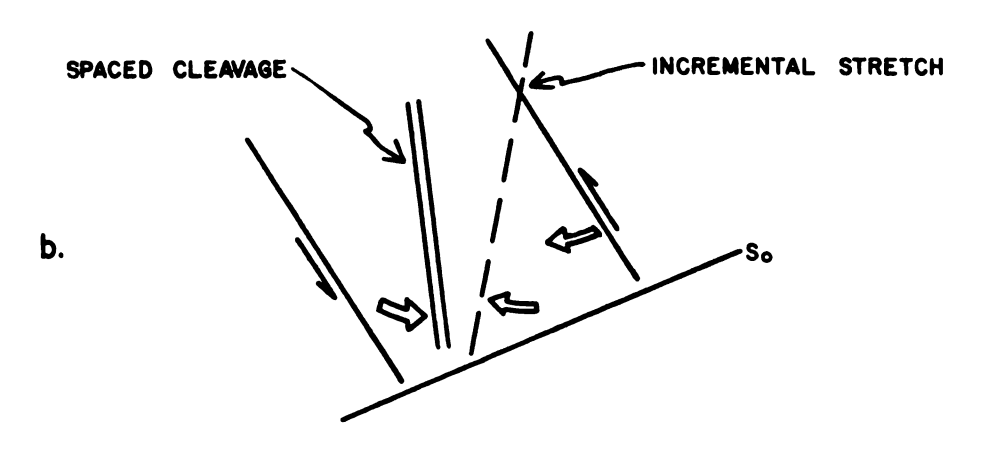
within that plane. If special conditions are specified, i.e., a coaxial strain history and mass transfer across the cleavage surfaces, it is possible that the slaty cleavage may track the XY-plane of the finite strain ellipsoid at all times (Williams, 1976a). The problem regarding the textural changes in response to changes in elongation direction within the slaty cleavage (XY-plane) has not been addressed.

It is instructive at this point to speculate as to what may be expected to occur during continued folding within the model of deformation described above. Assume that the maximum compression direction and the orientation of the slaty cleavage remain fairly constant. The spaced cleavage will continue to rotate (a rotation enhanced by the modelled shear couple) attaining progressively shallower dip angles to the northeast. As the angle between the maximum compression direction and the spaced cleavage decreases, the deviation of the expected shear plane from that predicted by the Coulomb theory increases. The shear plane therefore steepens, i.e., rotates toward the orientation of the spaced cleavage (Figure 26). It is apparent that the spaced cleavage may become the shear plane long before it has been tilted to a 45° angle with the maximum compression direction. Shear on the spaced cleavage planes is then expected to crenulate the by now well-developed slaty cleavage into asymmetric folds. In such a sequence of events the resulting crenulation cleavage would clearly not represent the XY-plane of finite strain nor would it be attributable to a separate deformation episode.

The overprinting relationships of crenulation cleavages on a domainal microfabric at a much smaller scale (e.g., slaty cleavage) have commonly been described and various mechanisms have been proposed (Hoeppener, 1956; Cosgrove, 1976; Hobbs et al., 1976; Williams, 1976b; Gray, 1977; Marlow et al., 1977; Gray et al., 1979). These mechanisms include shear in a direction parallel



SSW



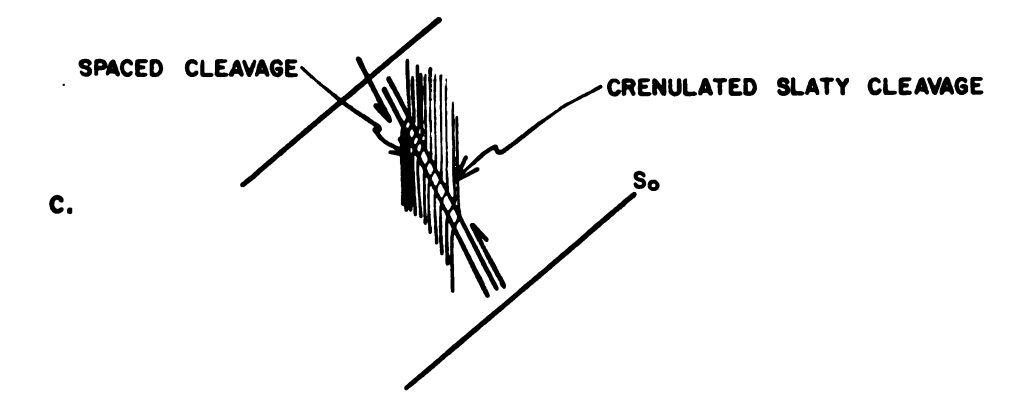


FIGURE 26 SCHEMATIC DIAGRAM ILLUSTRATING THE KINEMA-TICS OF THE HYPOTHETICAL MODEL FOR THE FORMATION OF A CRENULATION CLEAVAGE.

to the resulting crenulation cleavage, the development of buckling instabilities in the "primary" deformational fabric and/or solution-redeposition processes. Williams et al. (1981) point out that shearing parallel to the foliation cannot produce axial planar crenulation cleavage. Within the hypothetical model described herein, the spacing and morphology of the initial spaced cleavage would control the initiation of a crenulation cleavage by shear along discrete surfaces.

Implications for the Deformation of the Marquette Trough

The significance of the results of this study for a model of the deformation of the Marquette Trough will be briefly discussed regarding: 1) the orientation of the strain axes, and 2) the local and regional strain gradients.

The orientation of the principal flattening direction, northeast-southwest, contrasts with that found by Westjohn (1978) who reported shortening in a north-south direction. In his study he sampled primarily rocks from the central and eastern portions of the trough. This study locality is closer to the margin of the trough and it can be expected that the depth to the Archaean gneiss basement is also much less. The trough is bounded by steep basement faults along which movement took place during an initial rifting and subsidence phase (Cambray, 1978). The observed displacements along some of the steep, northwest-trending faults at the study locality are interpreted as arising from this tectonic phase.

It is unclear how the basement behaved during the deformation of the metasedimentary cover. Some of the steep faults may have become reactivated as reverse faults during the Penokean Orogeny and their trends reflected in the fold trends of the overlying metasediments. Toward the center of the Marquette Trough the effect of local variation in fault attitudes is masked by the greater thickness of the cover and the dominant flattening trend observed is north-south.

An increase in strain magnitudes can be demonstrated from the flat-lying to the folded layers (i.e., from south to north) at the study locality: 16% northeast shortening, 9% northwest shortening and 25% vertical extension (Table 3). The strain values reported by Westjohn (1978) are relative to an initial sphere. If these values are corrected to take into account the predeformational compactional strain calculated in this study, the strain magnitudes are about 75% north-south flattening, 15% east-west shortening and 100% vertical extension. Thus the regional strain gradient increasing from the southern margin of the trough toward the center is estimated as approximately 45% north-south flattening, 14% east-west shortening and 83% vertical extension.

Interpretation of a gravity profile across the Marquette Trough is in terms of differentially uplifted blocks of gneiss basement bounded by steep faults (Klasner et al., 1974). Because of the absence of a definable decollement surface between the metasedimentary cover and the gneiss basement, the latter must have undergone substantial deformation during the Penokean Orogeny. The involvement of the basement during the orogenic event is interpreted as indicating that stresses are propagated and transmitted by the basement and may have originated within it. The above arguments are inconsistent with the models of Cannon (1973) and Klasner (1978) and lend strong support to Cambray's (1978) plate tectonic model for the Marquette Trough.

CONCLUSION

From the finite strain data presented the following conclusions may be made: 1) The predeformational shape of the reduction spots in the argillite and slate studied is clearly not spherical but oblate, flattened in the bedding plane. Shortening of such an ellipsoid will lead to constrictional strains before a flattening strain state is attained (Figure 25). 2) Considering the directional error of the strain axes, about 5°, the slaty cleavage is parallel to the XY-plane of the strain ellipsoid calculated from reduction spots. The reduction spot strain ellipsoid is a mean ellipsoid derived from a large number of reduction spots with a considerable scatter of orientations (Figure 20). Assuming that the slaty cleavage represents the XY-plane of strain of individual reduction spots may thus lead to considerable error in the calculated strain, an error which is expected to decrease with increasing strain. In addition, the derived strain magnitudes need to be corrected for compactional strains. 3) The quartz grain shape fabric in the quartzites is statistically random indicating that the shape fabric does not record the reduction spot strains calculated for argillites from comparable domains. It is tentatively suggested that intergranular deformation (grain-boundary sliding) and brittle failure on joints with accompanying mass transfer may have accommodated a significant amount of strain.

The modelling of the progressive deformation of the reduction spots at the study locality resulted in the following sequence: 1) 40% gravitational compaction, 2) 30% layer parallel flattening prior to folding, 3) additional pure shear of 15% subhorizontal shortening and simple shear on a northeast-dipping, progressively steepening shear plane. The vertical north-south trending joints in

the quartzite layers may reflect extension subparallel to the fold axis during strain increment (2).

Based on the modelling of the reduction spot finite strain states and the orientation of cleavage lineations, the spaced cleavage formed earlier than the slaty cleavage. Theoretical arguments consistent with the modelling lead to the hypothesis that the spaced cleavage may become a favourable shear plane as folding continues and subsequently a crenulation cleavage. Although speculative, such considerations are of importance regarding models for the initiation of a crenulation cleavage and, the significance of superimposed cleavages as indicators of single or multiple deformation events.

The northwest trend of the large-scale fold and the horizontal northeast-trending shortening direction at the study locality differ from the overall north-south flattening of the Marquette Trough. It is proposed that the proximity of the study locality to the margin of the trough and to the basement causes the fold trends to be strongly influenced by local variations in the attitude of basement faults presumably active during deformation of the metasediments. That the Penokean Orogeny involved the basement is also inferred from the observed strain gradients across the Marquette Trough.

REFERENCES

- Borradaile, G. J., 1981. Particulate flow of rock and the formation of cleavage. Tectonophysics, v. 72, p. 305-321.
- Boulter, C. A., 1976. Sedimentary fabrics and their relation to strain analysis methods. Geology, v. 4, p. 141-146.
- Cambray, F. W., 1978. Plate tectonics as a model for the environment of sedimentation of the Marquette Supergroup and the subsequent deformation and metamorphism associated with the Penokean Orogeny (abstract). 24th Inst. Lake Superior Geology.
- Cannon, W. F., 1973. The Penokean Orogeny in northern Michigan. In Huronian Stratigraphy and Sedimentation (G. M. Young, ed). Geol. Assoc. Can. Spec. Paper 12, p. 251-271.
- Cannon, W. F. and Gair, J. E., 1970. A revision of stratigraphic nomenclature for Middle Precambrian rocks in northern Michigan. Geol. Soc. Am. Bull., v. 81, p. 2843-2846.
- Cosgrove, J. W., 1976. The formation of crenulation cleavage. J. Geol. Soc. Lond., v. 132, p. 155-178.
- Dunnet, D. and Siddans, A. W. B., 1971. Non-random sedimentary fabrics and their modification by strain. Tectonophysics, v. 12, p. 307-325.
- Elliott, D., 1970. Determination of finite strain and initial shape from deformed elliptical objects. Geol. Soc. Am. Bull., v. 81, p. 2221-2236.
- Flinn, D., 1962. On folding during three-dimensional progressive deformation. Quart. J. Geol. Soc. Lond., v. 118, p. 385-433.
- Gair, J. E. and Thadden, R. E., 1968. Geology of the Marquette and Sands Quadrangles, Marquette County, Michigan. U.S. Geol. Surv. Prof. Paper 397, 77p.
- Graham, R. H., 1978. Quantitative deformation studies in the Permian rocks of the Alpes-Maritimes. Proc. Symp. in Honour of Prof. J. Goguel (B.R.G.M.), p. 219-238.
- Gray, D. R., 1977. Differentiation associated with discrete crenulation cleavages. Lithos, v. 10, p. 89-101.
- Gray, D. R. and Durney, D. W., 1979. Crenulation cleavage differentiation: implications of solution-deposition processes. J. Struct. Geol., v. 1, p. 73-80.

- Hobbs, B. E.; Means, W. D. and Williams, P. F., 1976. An Outline of Structural Geology. J. Wiley and Sons, Inc., 571p.
- Hoeppener, R., 1956. Zum Problem der Bruchbildung, Schieferung und Faltung. Geol. Rundsch, v. 45, p. 247-283.
- Holst, T. B., 1982. The role of initial fabric on strain determination from deformed ellipsoidal objects. Tectonophysics, v. 82, p. 329-350.
- Jaeger, J. C., 1960. Shear failure of anisotropic rocks. Geol. Mag., v. 97, p. 65-72.
- Klasner, J. S., 1978. Penokean deformation and associated metamorphism in the western Marquette Range, northern Michigan. Geol. Soc. Am. Bull., v. 89, p. 711-722.
- Klasner, J. S. and Cannon, W. F., 1974. Geologic interpretation of gravity profiles in the western Marquette district, northern Michigan. Geol. Soc. Am. Bull., v. 85, p. 213-218.
- Larue, D. K., 1981. The Chocolay Group, Lake Superior region, U.S.A.: Sedimentologic evidence for deposition in basinal and platform settings on an Early Proterozoic craton. Geol. Soc. Am. Bull., pt. 1, v. 92, p. 417-435.
- Larue, D. K. and Sloss, L. L., 1980. Early Proterozoic sedimentary basins of the Lake Superior region. Geol. Soc. Am. Bull., pt. II, v. 91, p. 1836-1874.
- Lisle, R. J., 1979. Strain analysis using deformed pebbles: the influence of initial pebble shape. Tectonophysics, v. 60. p. 263-277.
- Marlow, P. C. and Etheridge, M. A., 1977. Development of layered crenulation cleavage in mica schists of the Kanmantoo Group near Macclesfield, South Australia. Geol. Soc. Am. Bull., v. 88, p. 873-882.
- Matthews, P. E.; Bond, R. A. B. and Van Den Berg, J. J., 1974. An algebraic method of strain analysis using elliptical markers. Tectonophysics, v. 24, p. 31-67.
- Miller, D. N. and Folk, R. L., 1955. Occurrence of detrital magnetite and ilmenite in red sediments: new approach to significance of redbeds. Bull. Am. Assoc. Petrol. Geol., v. 39, p. 338-345.
- Miller, D. M. and Oertel, G., 1979. Strain determination from the measurement of pebble shapes: a modification. Tectonophysics, v. 55, p. T11-T13.
- Nicolas, A. and Poirier, J. P., 1976. Crystalline plasticity and solid state flow in metamorphic rocks. J. Wiley and Sons, Inc., 437p.
- O'Brien, N. R., 1970. The fabric of shale an electron-microscope study. Sedimentology, v. 15, p. 229-246.
- Oertel, G., 1978. Strain determination from the measurement of pebble shapes. Tectonophysics, v. 50, p. T1-T7.

- Ramberg, H., 1964. Selective buckling of composite layers with contrasted rheological properties, a theory for simultaneous formation of several orders of folds. Tectonophysics, v. 1, p. 307-341.
- Ramsay, J. G., 1967. Folding and Fracturing of Rocks. McGraw-Hill Book Co., 568p.
- Ramsay, J. G. and Wood, D. S., 1973. The geometric effects of volume change during deformation processes. Tectonophysics, v. 16, p. 263-277.
- Rieke, H. H., III and Chillingarian, G. V., 1974. Compaction of argillaceous sediments: Developments in Sedimentology, v. 16. Elsevier, 424p.
- Seymour, D. B. and Boulter, C. A., 1979. Tests of computerized strain analysis methods by the analysis of simulated deformation of natural unstrained sedimentary fabrics. Tectonophysics, v. 58, p. 221-235.
- Sherwin, J. A. and Chapple, W. M., 1968. Wavelengths of single layer folds: a comparison between theory and observation. Am. J. Sci., v. 266, p. 167-179.
- Shimamoto, T. and Ikeda, Y., 1976. A simple algebraic method for strain estimation from deformed ellipsoidal objects. 1. Basic theory. Tectonophysics, v. 36, p. 315-337.
- Siddans, A. W. B., 1980. Analysis of three-dimensional, homogeneous, finite strain using ellipsoidal objects. Tectonophysics, v. 64, p. 1-16.
- Sims, P. K.; Card, K. D.; Morey, G. B. and Peterman, Z. E., 1980. The Great Lakes tectonic zone a major crustal structure in central North America. Geol. Soc. Am. Bull., pt. 1, v. 91, p. 690-698.
- Skempton, A. W., 1970. The consolidation of clays by gravitational compaction. Q. J. Geol. Soc. Lond., v. 125, p. 373-411.
- Taylor, G. L., 1972. Stratigraphy, sedimentology and sulphide mineralization of the Kona Dolomite. Unpublished Ph.D. Thesis, Michigan Technological University, Houghton, Michigan.
- Tullis, D. E. and Wood, D. S., 1975. Correlation of finite strain from both reduction bodies and preferred orientation of micas in slate from Wales. Geol. Soc. Am. Bull., v. 86, p. 632-638.
- Van Hise, C. R. and Bayley, W. S., 1897. The Marquette iron-bearing district of Michigan. U.S. Geol. Surv. Monograph 28, 608p.
- Van Schmus, W. R., 1976. Early and Middle Proterozoic history of the Great Lakes area, North America. Phil. Trans. R. Soc. Lond., v. A280, p. 605-628.
- Walsh, J. B. and Brace, W. F., 1964. A fracture criterion for brittle anisotropic rock. J. Geophys. Res., v. 69, p. 3449-3456.

- Westjohn, D. B., 1978. Finite strain in the Precambrian Kona Formation, Marquette County, Michigan. Unpublished M.S. Thesis, Michigan State University, East Lansing, Michigan, 72p.
- White, S., 1976. The effects of strain on the microstructures, fabrics, and deformation mechanisms in quartzites. Phil. Trans. R. Soc. Lond., v. A283, p. 69-86.
- Williams, P. F., 1976a. Relationships between axial plane foliations and strain. Tectonophysics, v. 30, p. 181-196.
- Williams, P. F., 1976b. Foliation: a review and discussion. Tectonophysics, v. 39, p. 305-328.
- Williams, P. F. and Schoneveld, Chr., 1981. Garnet rotation and the development of axial plane crenulation cleavage. Tectonophysics, v. 78, p. 307-334.
- Wood, D. S., 1973. Patterns and magnitudes of natural strain in rocks. Phil. Trans. R. Soc. Lond., v. A274, p. 373-382.
- Wood, D. S., 1974. Current views of the development of slaty cleavage. <u>In Ann.</u> Rev. Earth Planet. Sci., v. 2, p. 269-401.
- Wood, D. S. and Oertel, G., 1980. Deformation in the Cambrian slate belt of Whales. J. Geol., v. 88, p. 309-326.

APPENDIX. ERROR ANALYSIS OF FINITE STRAIN DETERMINATIONS.

The errors arising from field and laboratory measurements limit the accuracy of the strain values and orientations. A rigorous statistical evaluation of these errors was not attempted due to the somewhat unorthodox methods used. The following analysis yields maximum estimates of the uncertainties introduced by the measurements.

Errors in the Strain Determination from Quartz Grain Shapes

a.	Orientation of sample in the field	± 2°
b.	Transfer of orientation to sample plane: goniometer measurements equal-area stereonet	± ½° ± 1°
c.	Transfer of orientation from the thin section onto the photograph	± 1°
d.	Determination of axes orientation	± 1°
e.	Determination of axes length	± .05 units

For the following calculated parameters, the uncertainties introduced by these errors have been derived:

Orientation of center point, $\overline{\theta}$	± 7 ⁰
Radius vector to center point, $\overline{\epsilon}$	± .03
Strain ratio at center point, \overline{S}	± .08

Errors in the Strain Determination from Reduction Spots

a.	Orientation of sample in the field	± 2°
b.	Transfer of orientation to sample plane: goniometer measurements equal-area stereonet	± ½° ± 1°
c.	Orthogonality of cut slab sets	± ½°
d.	Determination of axes orientation	± 1/2°
	The error may be as high as ± 3° for ellipses of low axial ratios.	
e.	Determination of axes length	± .05 units

Based on these estimates the maximum error in the orientation of the axes on a given plane, before input into the computer program, is about $\pm 5^{\circ}$. Considering systematic errors negligible, the error reported for the orientation of the three-dimentional strain axes is $\pm 5^{\circ}$. The error of $\pm 5^{\circ}$ for the orientation of the axes introduces an average error of about 1% for the magnitude of the plane tensors. The error reported for the magnitude of the three-dimentional strain axes consists of 1% measurement error plus the computer-calculated standard deviation.

